Article

Cell Reports

Mycobacterium tuberculosis Limits Host Glycolysis and IL-1β by Restriction of PFK-M via MicroRNA-21

Graphical Abstract

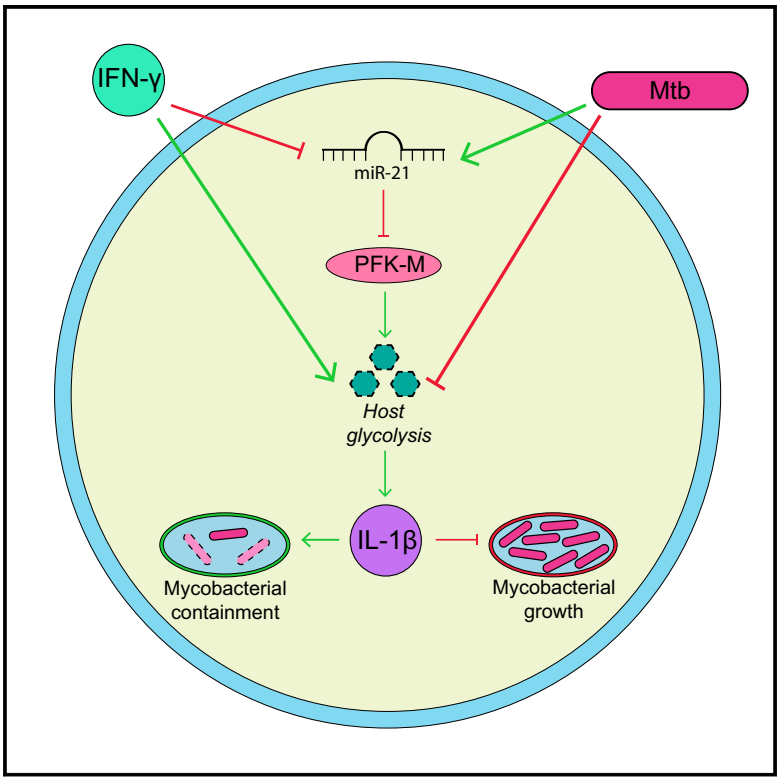

Authors

Emer E. Hackett, Hugo Charles-Messance, Seónadh M. O'Leary, ..., Stephen V. Gordon, Joseph Keane, Frederick J. Sheedy

Correspondence

fsheedy@tcd.ie

In Brief

Hackett et al. identify a role for the anti-inflammatory miR-21 in limiting host glycolysis during tuberculosis (TB) infection to favor bacterial replication. This occurs by targeting a pro-glycolytic isoform at the rate-limiting step in glycolysis, PFK-M, a process antagonized by the host Th1-cytokine IFN-γ, to promote full macrophage activation and antimicrobial function.

Highlights

- Mtb infection of macrophages limits metabolic reprogramming over time
- Glycolysis is limited through sustained induction of anti-inflammatory miR-21
- PFK-M is a miR-21 target gene
- IFN-γ promotes glycolysis by targeting miR-21

Hackett et al., 2020, Cell Reports *30*, 124–136
January 7, 2020
https://doi.org/10.1016/j.celrep.2019.12.015

CellPress

OPEN ACCESS
CellPress

Cell Reports
Article

Mycobacterium tuberculosis Limits Host Glycolysis and IL-1β by Restriction of PFK-M via MicroRNA-21

Emer E. Hackett,[1] Hugo Charles-Messance,[1] Seónadh M. O'Leary,[2] Laura E. Gleeson,[2] Natalia Muñoz-Wolf,[1] Sarah Case,[1] Anna Wedderburn,[1] Daniel G.W. Johnston,[1] Michelle A. Williams,[3] Alicia Smyth,[4] Mireille Ouimet,[6] Kathryn J. Moore,[6] Ed C. Lavelle,[1] Sinéad C. Corr,[3] Stephen V. Gordon,[4] Joseph Keane,[2] and Frederick J. Sheedy[1,5,7,*]

[1]School of Biochemistry and Immunology, Trinity College, Dublin 2, Ireland
[2]School of Medicine, Trinity College, Dublin 2, Ireland
[3]School of Genetics and Microbiology, Trinity College, Dublin 2, Ireland
[4]School of Veterinary Medicine and Conway Institute, University College Dublin, Dublin, Ireland
[5]Conway Institute, University College Dublin, Dublin, Ireland
[6]School of Medicine, New York University, New York, NY, USA
[7]Lead Contact
*Correspondence: fsheedy@tcd.ie
https://doi.org/10.1016/j.celrep.2019.12.015

SUMMARY

Increased glycolytic metabolism recently emerged as an essential process driving host defense against *Mycobacterium tuberculosis* (Mtb), but little is known about how this process is regulated during infection. Here, we observe repression of host glycolysis in Mtb-infected macrophages, which is dependent on sustained upregulation of anti-inflammatory microRNA-21 (miR-21) by proliferating mycobacteria. The dampening of glycolysis by miR-21 is mediated through targeting of phosphofructokinase muscle (PFK-M) isoform at the committed step of glycolysis, which facilitates bacterial growth by limiting pro-inflammatory mediators, chiefly interleukin-1β (IL-1β). Unlike other glycolytic genes, PFK-M expression and activity is repressed during Mtb infection through miR-21-mediated regulation, while other less-active isoenzymes dominate. Notably, interferon-γ (IFN-γ), which drives Mtb host defense, inhibits miR-21 expression, forcing an isoenzyme switch in the PFK complex, augmenting PFK-M expression and macrophage glycolysis. These findings place the targeting of PFK-M by miR-21 as a key node controlling macrophage immunometabolic function.

INTRODUCTION

Reprogramming of cellular metabolism has emerged as a directive mechanism controlling responses in immune cells (Pearce and Pearce, 2013). In particular, macrophages display an increased reliance on the glycolytic pathway during inflammatory activation (Jha et al., 2015; Rodríguez-Prados et al., 2010). This is linked to pro-inflammatory processes, including cytokine production (Tannahill et al., 2013), antigen presentation (Everts et al., 2014), and containment of bacteria (Garaude et al., 2016). We recently demonstrated the importance of glycolysis in host defense against the intracellular pathogen *Mycobacterium tuberculosis* (Mtb) (Gleeson et al., 2016, 2018), which has evolved to replicate within macrophages of the pulmonary compartment (Huang et al., 2018). Failure to contain mycobacteria results in the development of tuberculosis, both latent and active infections, which, coupled with increasing drug resistance and ineffective vaccines, has caused a global health crisis (O'Garra et al., 2013). Exploiting metabolic reprogramming through manipulation of nutrients or by repurposing of existing drugs will impact the development of novel immunotherapies and improved vaccines.

While several studies have documented increased glycolysis in Mtb-infected macrophages (Braverman et al., 2016; Gleeson et al., 2016; Huang et al., 2018; Lachmandas et al., 2016a, 2016b), alongside the reprogramming of other metabolic pathways, including lipid metabolism (Knight et al., 2018; Ouimet et al., 2016; Russell et al., 2009), little is known about how these pathways are regulated during infection and whether they play a role in defective immunity leading to disease. Additionally, macrophage ontogeny is known to affect immunometabolic responses, although the mechanisms controlling this remain unclear (Gleeson et al., 2018; Huang et al., 2018). Non-coding RNAs, particularly microRNAs (miRNAs), are important regulators of macrophage activation and innate immunity (Graff et al., 2012). miRNA-21 (miR-21) is one of the most highly expressed miRNAs in myeloid cells and emerged as an anti-inflammatory miRNA (Sheedy, 2015). We previously demonstrated that miR-21 is induced by TLR4 signaling to promote interleukin-10 (IL-10) production by limiting PDCD4 protein (Sheedy et al., 2010), and other groups have implicated this in efferocytosis, alongside negative regulation of tumor necrosis factor (TNF) by targeting PTEN protein (Das et al., 2014). Dendritic cell activation and subsequent T cell function is also limited by miR-21 by targeting IL-12p35 mRNA (Lu et al., 2011). Expression of miR-21 has been reported in various cellular models of mycobacterial infection (Kumar et al., 2012; Wu et al., 2012) and importantly was associated with dormancy in *Mycobacterium leprae* lesions through negative regulation of multiple pro-inflammatory processes (Liu et al., 2012). However, its role in cellular metabolic programming is not known.

Since Mtb infection is known to favor the development of anti-inflammatory macrophages and evades pro-inflammatory

mechanisms (O'Garra et al., 2013), we hypothesized that it would also evade host immunometabolic responses. Interestingly, we observe that persistent Mtb infection of macrophages was associated with negative regulation of host glycolysis, and this was dependent on the induction of miR-21. Our data indicate that Mtb replication in macrophages was driven by suppression of metabolic reprogramming and associated IL-1β production through miR-21. Crucially, we found that the specific control of glycolysis in Mtb-infected cells occurred through repression of a novel miR-21 target at the rate-limiting and committed step of glycolysis (Tanner et al., 2018), the phosphofructokinase muscle (PFK-M) isoform, whose expression is dynamically regulated during Mtb infection to evade inflammation and in macrophage activation by interferon-γ (IFN-γ), to drive pro-inflammatory responses. Collectively, these data suggest that Mtb alters macrophage immunometabolic programming via miR-21 to ensure survival and replication.

RESULTS

Mtb Infection Attenuates Metabolic Reprogramming and Drives Anti-Inflammatory miR-21

To further explore the mechanisms underlying metabolic reprogramming during Mtb infection, we treated bone-marrow-derived macrophages (BMDMs) with equivalent amounts of heat-killed Mtb (hk-Mtb) H37Ra or viable bacillus. Interestingly, we observed that hk-Mtb caused sustained accumulation of extracellular lactate over 72 h similar to lipopolysaccharide (LPS) treatment, indicative of increased glycolysis, whereas the viable bacillus was unable to induce lactate production to the same extent (Figure 1A). This was associated with reduced ability of viable Mtb to promote IL-1β production, despite triggering similar TNF production (Figures S1A and S1B) and reduced induction of pro-glycolytic genes after 24 h infection, including *Slc2a1* (which encodes the glucose transporter GLUT1), hexokinase-2 (*Hk2*; which encodes the primary step in glycolysis), and lactate dehydrogenase-A (*LdhA*), the final glycolytic step for lactate production (Figure 1B). A similar trend was observed when BMDMs were infected with virulent Mtb H37Rv, with reduced lactate accumulation observed in cells infected with equivalent amounts of attenuated H37Ra or virulent H37Rv Mtb strains (ranging from 2 to 5 bacteria per cell), relative to a top dose of inactivated forms of each strain (iMtb; hk-Mtb for H37Ra or γ-irradiated Mtb [γMtb] for H37Rv) (Figure 1C). A similar trend was observed in human cells when human-monocyte-derived macrophages (hMDMs; Figure S1C) were infected with equal amounts of viable Mtb H37Ra or hk-Mtb H37Ra (Figure 1D). To confirm that persistent infection with Mtb can attenuate macrophage metabolic reprogramming over time, we modeled the primary host cell for Mtb *ex vivo* (Huang et al., 2018). Human alveolar macrophages (hAMs) were isolated from donor bronchoalveolar lavage and infected *in vitro* with virulent Mtb H37Rv or γMtb H37Rv, alongside LPS treatment. Again, treatment with the inactive form was superior at inducing *IL1B* mRNA, although both forms induced similar *TNF* mRNA, which decreases over time (Figure 1E). As previously observed (Gleeson et al., 2018), γMtb promoted the induction *SLC2A1* and *HK2,* while live Mtb infection is a poor inducer of these (Figure 1E). No induction of *LDHA* was observed in these cells. Our results are supported by a recent report examining macrophage bioenergetics and the accumulation of glycolytic intermediates after virulent Mtb infection (Cumming et al., 2018) and together demonstrate that infection with Mtb, which adapts and grows within macrophages over time, negatively regulates the induction of glycolysis in macrophages.

To promote its own survival within macrophages, Mtb is known to induce anti-inflammatory mediators, including IL-10 (Flynn et al., 1995; Pitt et al., 2012), which has been linked to negative regulation of glycolysis (Ip et al., 2017). However, we did not observe enhanced IL-10 production in BMDMs infected with live Mtb (H37Ra or H37Rv) relative to inactivated forms, despite reduced IL-1β (Figures S1D–S1J). We next examined the expression of another anti-inflammatory mediator linked to IL-10 production, the miRNA miR-21 (Sheedy et al., 2010). Notably, we observed dose-dependent induction of the bioactive mature miR-21 in both BMDMs and hMDMs treated with increasing hk-Mtb or viable Mtb (Figures 1F and 1G), with viable Mtb inducing significantly more miR-21 than equivalent amounts of hk-Mtb (Figures 1F and 1G). This is preceded by early induction of the primary miR-21-containing transcript, *pri-miR-21* (Figure 1H, 3–24 h post-infection), implying elevated transcriptional upregulation by live Mtb infection. A similar trend was observed when BMDMs were infected with virulent or attenuated Mtb strains (H37Ra or H37Rv), with viable forms of both similarly driving enhanced mature miR-21 levels relative to inactivated forms 72 h post-infection (Figure 1I), with similar kinetics of *pri-miR-21* and mature miR-21 appearance (Figure S1K). A similar effect was observed in hAMs with early upregulation of *pri-miR-21* preceding accumulation of mature miR-21 (Figure 1J). Furthermore, lung tissue from mice infected *in vivo* with Mtb (Erdman strain) shows upregulation of *pri-miR-21* at 30 days post-infection, which is maintained up to 53 days post-infection (Figure 1K), indicative of an important role for miR-21 during chronic Mtb infection.

miR-21 Limits Glycolysis during Mtb Infection

To investigate whether miR-21 impacts macrophage metabolism during Mtb infection, we utilized a mouse model of macrophage miR-21-deficiency. We isolated BMDM from wild-type (WT) and miR-21 *loxP*-targeted mice (Johnston et al., 2017) and confirmed similar numbers of CD11b-F4/80 double-positive cells (Figure S2A). In resting miR-21-deficient BMDMs, both primary and mature miR-21 were undetectable and LPS-induced upregulation of both transcripts was impaired, while levels of neighboring *Tmem49* gene were unaffected (Figure S2B). Functionally, *MiR-21*$^{-/-}$ BMDMs express higher levels of miR-21 targets, *Pdcd4* and *Pten* mRNA, before and after LPS treatment, and consistent with earlier work (Sheedy et al., 2010) show impaired IL-10 production during TLR4 signaling (Figures S2B and S2C). Upon infection with a moderate MOI (5 bacteria per cell) of Mtb H37Ra, we found that the production of lactate over time was dramatically enhanced in *MiR-21*$^{-/-}$ BMDMs (Figure 2A), although uptake of bacteria at 3 h was similar between the two genotypes (Figures S2D and S2E). Enhanced lactate production was also observed when *MiR-21*$^{-/-}$ BMDMs were infected with virulent Mtb H37Rv (Figure 2B), which was not linked to altered viability, since similar amounts of cell death were

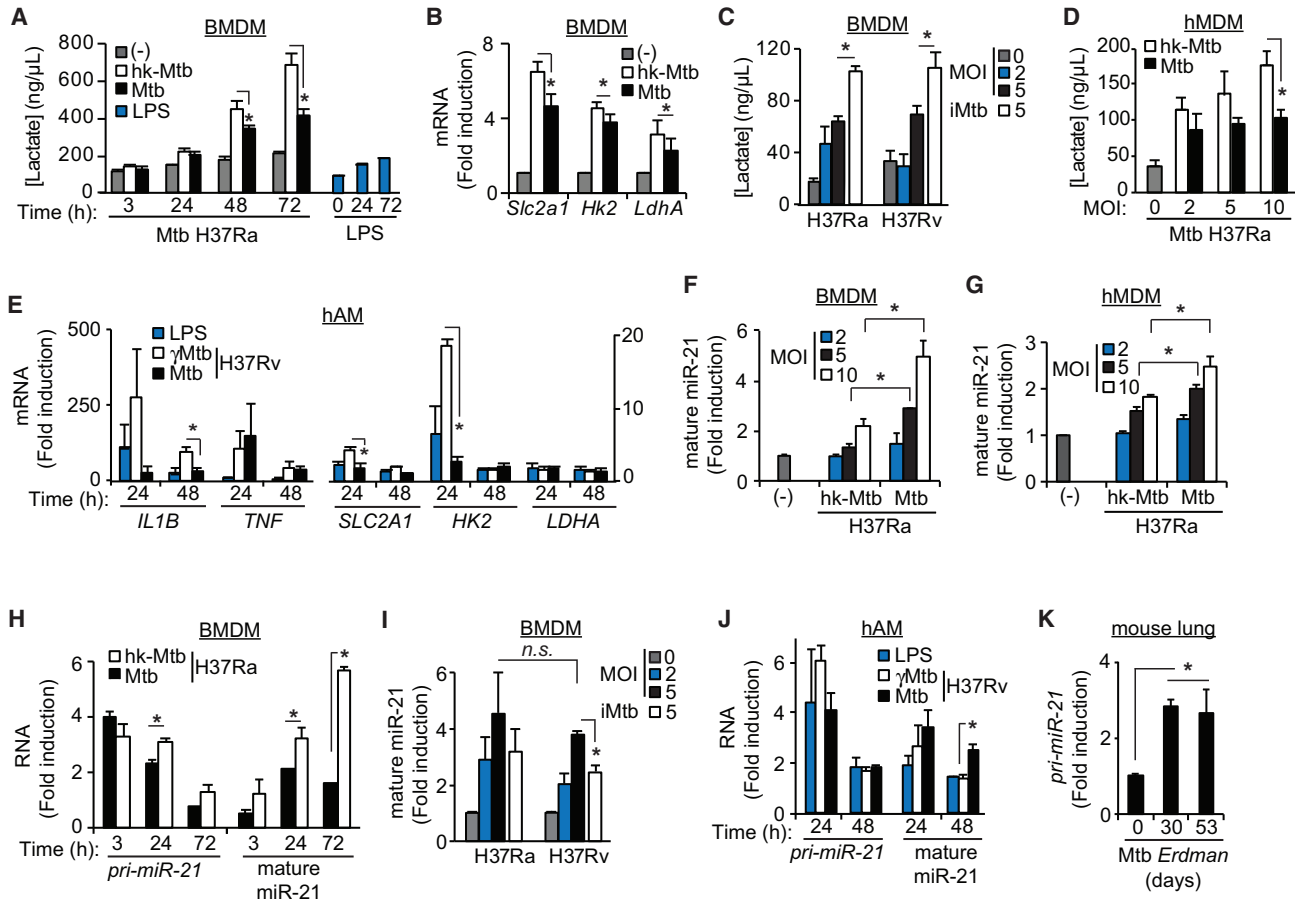

Figure 1. Mtb Infection Attenuates Macrophage Metabolic Reprogramming and Drives miR-21

(A) Extracellular lactate from bone-marrow-derived macrophages (BMDMs) infected with live *Mycobacterium tuberculosis* (Mtb) H37Ra or treated with heat-killed Mtb (hk-Mtb) H37Ra at an MOI of 5 bacteria per cell alongside LPS treatment (100 ng/mL) for the indicated times.

(B) qPCR of indicated genes in BMDMs treated as in (A) for 24 h.

(C) Extracellular lactate from BMDMs infected with viable Mtb H37Ra or H37Rv strains at indicated MOI or treated with hk-Mtb H37Ra or γ-irradiated Mtb H37Rv (MOI 5) for 24 h.

(D) Extracellular lactate from mature human-monocyte-derived macrophages (hMDMs) infected with Mtb as in (A).

(E) qPCR analysis of the indicated genes in human alveolar macrophages (hAMs) treated with viable Mtb H37Rv (Mtb) or γ-irradiated form (γMtb) at MOI of 2 or LPS (100 ng/mL) for 24–48 h.

(F–H) qPCR of mature miR-21 or primary miR-21 transcript (*pri-miR-21*) in BMDMs (F and H) or hMDMs (G) treated with hk-Mtb or infected with viable Mtb H37Ra (Mtb) at the indicated MOI for 24 h (F and G) or at MOI of 5 for various times (0–72 h; H).

(I) qPCR of mature miR-21 in BMDMs treated as in (C) for 72 h.

(J) qPCR of the indicated RNA species in hAMs treated as in (E).

(K) qPCR of *pri-miR-21* expression in lung tissue from mice infected with Mtb (Erdmann strain) for the indicated time (days).

Data represent mean concentration ± SEM for n = 3 independent experiments (A, C, and D) and mean fold-induction over uninfected cells ± SEM for n = 3 (B, G, and I) or n = 5 (F and H) independent experiments, n = 4 donors (E and J), or n = 5 mice (K). *p < 0.05; n.s., p > 0.05 for the indicated group comparisons (ANOVA with post hoc Tukey tests).

observed across both genotypes, as measured using a secreted lactate dehydrogenase (LDH) assay (Figure S2F). To validate the impact of miR-21 on glycolysis, we ablated miR-21 expression using antisense oligonucleotides in hMDMs. Reduction of basal and induced miR-21 by anti-miR-21 transfection was confirmed by qPCR (Figure S2G). Silencing of miR-21 in hMDMs increased lactate accumulation over the course of Mtb H37Ra infection, suggestive of increased glycolysis, and was similarly augmented in response to treatment with LPS or γMtb (Figure 2C). While infection with Mtb H37Ra drives the induction of pro-glycolytic genes (e.g., *Slc2a1*, *Hk2*, and *LdhA*) in BMDMs in a dose-dependent fashion to similar levels as LPS treatment, expression of these genes is enhanced in miR-21-deficient cells (Figure 2D). Enhanced induction of *Slc2a1* and *LdhA* mRNA was also observed in miR-21-deficient BMDMs after infection with the Mtb H37Rv strain (Figure S3A). These data suggest that miR-21 limits macrophage metabolic reprogramming during Mtb infection.

To confirm the role of miR-21 in regulating the macrophage bioenergetic response, we performed extracellular flux analysis

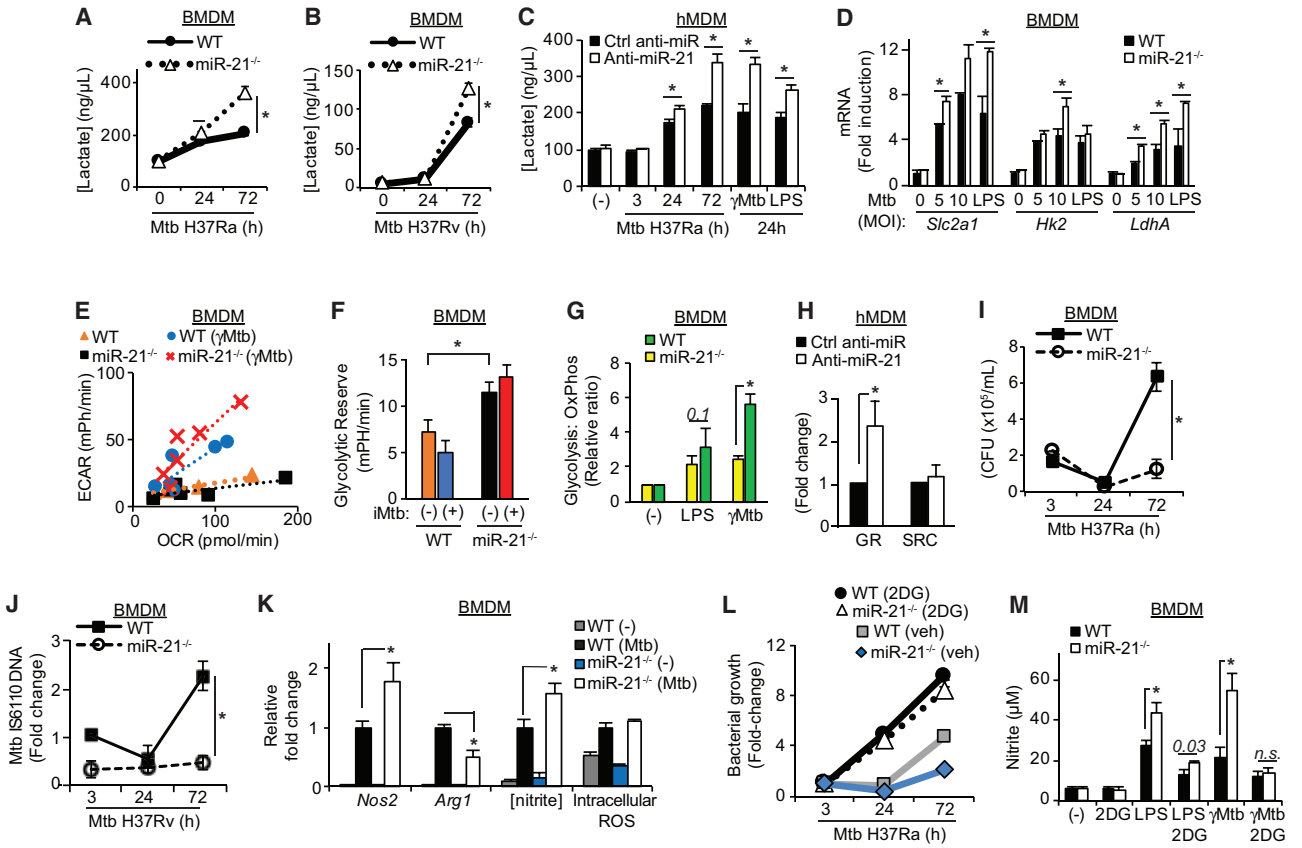

Figure 2. Restraint of Glycolysis by miR-21 Permits Mtb Growth in Macrophages

(A–C) Extracellular lactate from wild-type (WT) or miR-21-deficient (*miR-21*$^{-/-}$) BMDMs infected with Mtb H37Ra (A) or Mtb H37Rv (B) (MOI 5) for indicated times or hMDMs transfected with 50 nM miR-21-specific antisense (anti-miR-21) or a control nonspecific antisense (anti-miR-Ctrl) prior to infection with Mtb H37Ra (MOI 5, indicated times) or treated with γMtb (MOI 5) or LPS (100 ng/mL) for 24 h (C).

(D) qPCR of indicated genes in BMDMs infected with Mtb H37Ra at the indicated MOI or treated with LPS (100 ng/mL) for 24 h.

(E) Metabolic flux analysis of basal metabolism in untreated or γMtb-treated BMDMs (indicated genotype, MOI 5, 24 h) by measurement of extracellular acidification rate (ECAR) and oxygen consumption rate (OCR).

(F) Glycolytic reserve (GR) of untreated or γMtb-treated BMDMs (genotype indicated) treated with the indicated metabolic manipulations (Glu, addition of glucose; OM, oligomycin [1 μM], FCCP [1 μM], and rotenone + antimycin A [0.5 μM]).

(G) ECAR:OCR ratio in BMDMs treated with γMtb (MOI 5) or LPS (100 ng/mL) for 24 h.

(H) GR and spare respiratory capacity (SRC) of resting hMDMs transfected as in (C) and treated with inhibitors as in (G).

(I) Bacterial colony-forming units (CFUs) in BMDMs infected with Mtb H37Ra (MOI 5) for the indicated times.

(J) qPCR of bacterial 1S6110 genomic DNA (gDNA) relative to 16 s ribosomal RNA (rRNA) in BMDMs infected with Mtb H37Rv (MOI 5) for the indicated times.

(K) Relative expression of indicated mediators in BMDMs infected with Mtb H37Ra (Mtb; MOI 5, 24 h).

(L) Bacterial CFUs in BMDMs treated with 2DG (10 mM) and subsequently infected with Mtb H37Ra (MOI 5) as before.

(M) Nitrite species in supernatants from BMDMs pretreated with 2DG (10 mM) and subsequently treated with γMtb (MOI 5) or LPS (100 ng/mL) for 24 h.

Data represent mean concentration ± SEM (A–C and M), mean fold-induction over uninfected cells ± SEM (D and J), mean fold-change ± SEM (F–H, K, and L), or mean CFUs ± SEM (I) for n = 3 independent experiments. Energy plot (E) presents mean values and (H) shows mean ± SEM from n = 5 independent experiments. *p < 0.05; n.s., p > 0.05 for the indicated group comparisons (ANOVA with post hoc Tukey tests or Student's t test in H).

in resting BMDMs and BMDMs treated with γMtb, since viable infection was not compatible with the exposed Seahorse system. While resting WT and *MiR-21*$^{-/-}$ BMDMs display similar levels of both extracellular acidification (indicative of glycolytic activity) and oxygen consumption (a readout of tricarboxylic acid [TCA]-cycle-fueled oxidative phosphorylation), challenge with γMtb resulted in greater extracellular acidification rate (ECAR) in *MiR-21*$^{-/-}$ BMDMs (Figure 2E). Although both ECAR and oxygen consumption rate (OCR) are similar across uninfected WT and *MiR-21*$^{-/-}$ BMDMs basally, when treated with oligomycin to block oxidative phosphorylation and allow maximal glycolysis, miR-21-deficient macrophages demonstrate a higher glycolytic reserve (GR) than WT cells (Figure 2F). Furthermore, although GR is normally decreased after challenge with γMtb as cells begin to adopt glycolysis basally, *MiR-21*$^{-/-}$ BMDMs retain a higher capacity for glycolysis than their WT counterparts (Figures 2F, S3B, and S3C). Uncoupling the mitochondrial membrane with FCCP allows maximal oxidative phosphorylation and calculation of spare respiratory capacity (SRC), which is not significantly altered across

genotypes basally. SRC decreases with γMtb treatment, and this is more pronounced in miR-21-deficient cells, consistent with a higher glycolytic potential (Figures S3D–S3F). However, the basal ratio of glycolysis relative to oxygen consumption shows a more pronounced shift toward glycolysis in *MiR-21*$^{-/-}$ BMDMs, particularly pronounced for γMtb treatment, compared to WT BMDM (Figure 2G). The increased potential for glycolysis was confirmed in hMDMs transfected with anti-miR-21, which showed enhanced GR, without affecting SRC (Figure 2H).

Restraint of Glycolysis through miR-21 Permits Mtb Growth in Macrophages

We next investigated how negative regulation of glycolysis by miR-21 impacts macrophage anti-mycobacterial responses. We observed similar levels of bacterial uptake in WT and miR-21-deficient macrophages by microscopy (Figures S2D and S2E) and measuring mycobacterial colony-forming units (CFUs) at 3 h post-infection (Figure S4A). However, at later time points, we noted a marked difference in the ability of macrophages to contain Mtb. Although WT BMDMs initially contain Mtb H73Ra, bacterial growth ensues at later times. *MiR-21*$^{-/-}$ BMDMs permitted significantly less Mtb growth, with similar CFU numbers as baseline (Figure 2I). Similar containment of virulent Mtb was observed in *MiR-21*$^{-/-}$ BMDMs when the viability of Mtb H37Rv was measured using bacterial-chromosome-specific probes as readouts of bacterial replication (Figure 2J). This method was validated by Mtb H37Ra experiments, which revealed similar patterns as detected by CFU methods, undetectable in cells treated with hk-Mtb (Figures S4B and S4C). The decreased intracellular mycobacterial growth observed by multiple methods suggested an increased capacity of *MiR-21*$^{-/-}$ BMDMs to respond to Mtb. Conversely, *MiR-21*$^{-/-}$ BMDMs displayed increased levels of pro-inflammatory mediators linked to bacterial containment, including *Nos2* mRNA, a consequent reduction in Mtb-induced *Arg1*, and more reactive nitrogen and oxygen species (Figure 2K). Similar effects were observed in miR-21-silenced hMDMs, with improved containment of Mtb H37Ra up to 5 days post-infection (Figure S4D). To ascertain if the increased ability of miR-21-deficient macrophages to contain Mtb is linked to elevated glycolysis, we poisoned glycolysis using an inhibitor of the first hexokinase-mediated step in glycolysis, 2-deoxyglucose (2DG; Figure S4E). Inhibition of glycolysis enhanced bacterial growth in WT BMDMs and abrogated the protective effect of miR-21 deficiency (Figures 2L and S4F). Importantly, 2DG also blocked the production of nitrite species in both WT and miR-21-deficient macrophages in response to LPS and γMtb treatment (Figure 2M), implying that the anti-microbial response in *MiR-21*$^{-/-}$ BMDMs is driven by increased glycolytic flux, which is normally limited by miR-21 induction.

Control of IL-1β Production by miR-21 Regulates Anti-Mtb Responses

To further investigate inflammatory responses suppressed by miR-21 regulation of glycolysis, we measured the production of various cytokines. Although miR-21 promotes IL-10 production in TLR4 signaling (Sheedy et al., 2010; Figure S5A), no significant difference in Mtb-induced IL-10 was observed in WT and miR-21-deficient macrophages, and addition of IL-10 to *MiR-21*$^{-/-}$ BMDMs did not restore mycobacterial growth to WT levels (Figures S5B and S5C). Furthermore, although Mtb-induced TNF production was enhanced in Mtb-H37Ra-infected *MiR-21*$^{-/-}$ BMDMs (Figures S5D and S5E), neutralizing this with a blocking antibody that augments bacterial growth in WT cells did not restore growth to WT levels in *MiR-21*$^{-/-}$ BMDMs or alter levels of lactate production (Figures S5F and S5G). We thus turned our attention to IL-1β, a cytokine central in host defense to Mtb and sensitive to changes in metabolism (Gleeson et al., 2016; Mayer-Barber et al., 2014). Levels of extracellular IL-1β increase at later times post-infection with both Mtb H37Ra and H37Rv, and we observed a marked enhancement of IL-1β production in response to Mtb infection in *MiR-21*$^{-/-}$ BMDMs relative to WT (Figure 3A), as well as in miR-21-silenced hMDMs (Figure 3B). Conversely, transfection of BMDMs with a miR-21 mimic reduced IL-1β secretion after Mtb H37Ra infection (Figure 3C), confirming the ability of miR-21 to modulate IL-1β responses. Notably, blocking IL-1β using a specific antibody that significantly increases mycobacterial growth in WT cells also increased mycobacterial growth in *MiR-21*$^{-/-}$ BMDMs, restoring growth to WT levels (Figure 3D).

Since IL-1β production is subject to multiple levels of regulation, we thus monitored the induction of *Il1b* mRNA in Mtb-infected macrophages and found this was significantly augmented by miR-21 deletion, particularly at later times post-infection, in H37Ra- and H37Rv-infected BMDMs (Figure 3E). This effect on *IL1B* mRNA is also observed in miR-21-silenced hMDMs (Figure S5H). Increased glycolysis in macrophages potentiates late *Il1b* transcription via HIF-1α (Palsson-McDermott et al., 2015; Tannahill et al., 2013), and therefore, we examined if increased flux through glycolysis was fueling the increased pro-inflammatory response in miR-21-deficient macrophages. Blocking glycolysis with 2DG abolished the increased *Il1b* mRNA levels in miR-21-deficient BMDM after Mtb infection or LPS treatment (Figure 3F), implicating general transcriptional induction of the *Il1b* gene as a key process regulated by miR-21. Similar results were obtained in miR-21-silenced hMDMs when glycolysis is circumvented by an alternative method, replacing glucose with galactose (Gohil et al., 2010; Figure 3G), similar to 2DG-treated *MiR-21*$^{-/-}$ BMDMs (Figure S5I). To confirm the *in vivo* impact of miR-21 on Mtb-induced inflammation, we monitored cytokine levels in the murine peritoneal cavity after local injection of hk-Mtb (Martin et al., 2009). A small but significant increase was observed in TNF levels in lavage fluid from *MiR-21*$^{-/-}$ mice, with a more pronounced effect observed on *in vivo* IL-1β production and no impact on IL-10 (Figure 3H). Thus, production of IL-1β is a key process fueled by glycolysis and targeted by miR-21 to impact the ability of macrophages to contain Mtb.

miR-21 Targets the Expression of the Glycolytic Enzyme PFK-M

To confirm that increased glycolysis is a cause and not a consequence of increased inflammatory activity in miR-21-deficient macrophages, we monitored the effect of IL-1β targeting on lactate production and observed similar levels in all cultures (Figure S6A). Curiously, when we measured extracellular glucose in

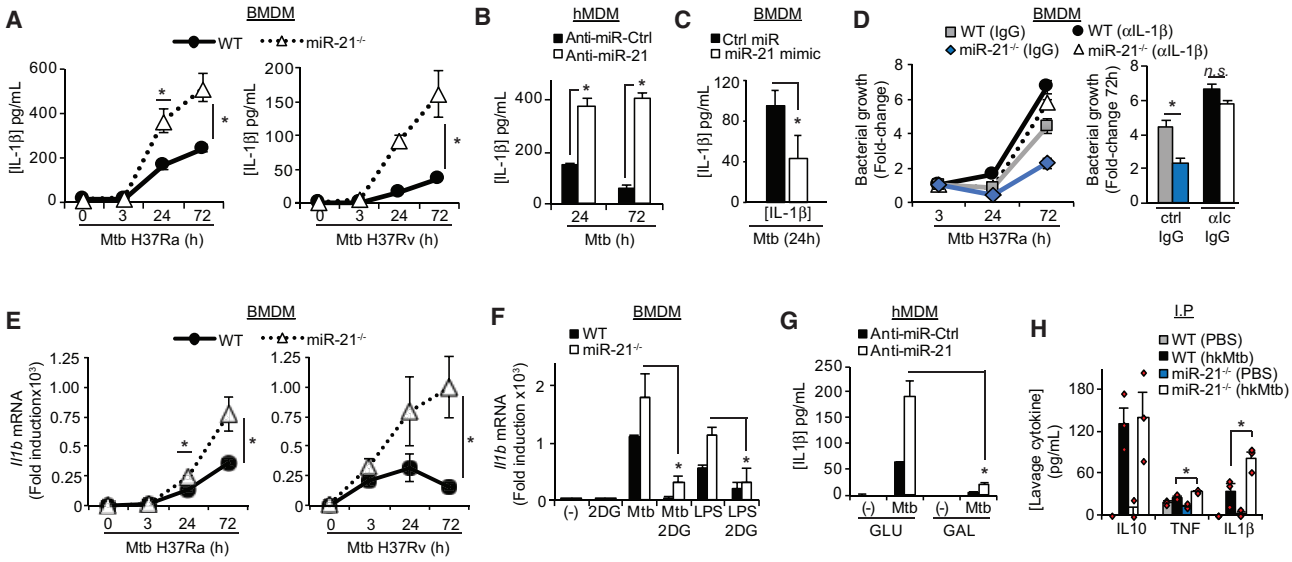

Figure 3. Control of IL-1β Production by miR-21 Regulates Anti-Mtb responses

(A and B) IL-1β ELISA in supernatants from BMDMs (genotype indicated) infected with Mtb H37Ra (A, left) or H37Rv (A, right) or hMDMs transfected with 50 nM miR-21-specific antisense (anti-miR-21) or a control nonspecific antisense (anti-miR-Ctrl) and subsequently infected with Mtb H37Ra (B) (MOI 5, indicated times).

(C) IL-1β ELISA in supernatants from BMDMs transfected with 50 nM of miR-21-specific mimic (miR-21 mimic) or a control nonspecific molecule (Ctrl-miR) infected with Mtb H37Ra (Mtb; MOI 5) for 24 h.

(D) Bacterial growth in BMDMs treated with anti-IL-1β specific antibody (αIL-1β; 1 μg/mL) or control immunoglobulin G (IgG) 3 h post-infection with Mtb H37Ra as in (A, left).

(E) qPCR of *Il1b* mRNA in BMDMs (genotype indicated) infected with Mtb H37Ra or H37Rv as before (A).

(F) qPCR of *Il1b* mRNA in BMDMs pretreated with 2DG (10 mM) infected with Mtb H37Ra (MOI 5) or treated with LPS (100 ng/mL) for 24 h.

(G) IL-1β ELISA in supernatants from hMDMs transfected as in (B) 24 h prior to infection with Mtb H37Ra (MOI 5, 24 h) in glucose-containing media (GLU) or glucose-free galactose-containing media (GAL).

(H) ELISA of indicated cytokines in lavage fluid taken from mice (genotype indicated) 24 h post-intraperitoneal injection of hk-Mtb (750 μg per mouse) or PBS. Data show mean concentration, fold-change in baseline CFUs (3 h) (A–C, G, and H) (D) and fold-induction over uninfected cells (E and F) and represent mean ± SEM for n = 4 (A, left panel) or n = 3 (A, right panel, B–G) independent experiments and for n = 3 mice per group (H). *$p < 0.05$; n.s., $p > 0.05$ for the indicated group comparisons (ANOVA with post hoc Tukey tests).

culture media, which decreases after infection due to increased metabolic activity (Figure S6B), we did not observe differences across genotypes, although *MiR-21*$^{-/-}$ BMDMs have increased glycolytic rates and produce more lactate. This suggested that the expression, and therefore activity, of a key process within the glycolytic pathway is directly impacted by miR-21. Although we previously observed increased induction of pro-glycolytic genes *Slc2a1*, *Hk2*, and *LdhA* in *MiR-21*$^{-/-}$ BMDMs (Figure 2D), these genes do not contain predicted binding sites for miR-21. Their enhanced production is likely a consequence of increased glycolytic activity activating HIF-1α (Palsson-McDermott et al., 2015), since this is abolished by 2DG treatment (Figure S6C).

We therefore performed *in silico* analysis of glycolytic genes and found an isoform of the committed step of glycolysis (Mor et al., 2011), PFK-M, which contains a predicted miR-21-binding site in its long 3′ UTR, conserved across multiple species including human and mouse. Other PFK isoforms (PFK-L [liver] and PFK-P [platelet]) have shorter 3′ UTRs and lack this sequence (Figure 4A). To confirm the potential for miR-21 to directly repress *PFK-M* expression, we cloned its 3′ UTR into a luciferase reporter. Plasmid-based overexpression of miR-21 dose-dependently decreases expression of the human *PFK-M* 3′ UTR-linked reporter by ~30% in both HEK293Ts and the macrophage cell line RAW267.4 (Figure 4B), with similar results obtained by co-transfection of miR-21 mimics (Figure S6D). This repression was lost when the predicted miR-21-site is mutated (Figure 4B). Consistent with metabolic reprogramming after infection or LPS activation of BMDMs, the expression of *Pfk-l* and *Pfk-p* isoforms was enhanced, with higher induced-*Pfk-l* levels in miR-21-deficient cells (Figure 4C). *Pfk-m*, however, displays a differential expression pattern and is not induced by Mtb infection in WT cells (Figure 4C). However, when miR-21 is absent, increased *Pfk-m* mRNA is observed after infection with both H37Ra and H37Rv Mtb strains (Figures 4C and 4D), supporting the notion that induction of miR-21 limits the expression of this isoform, which biochemical and genetic studies have suggested possesses an increased affinity for its substrate fructose-6-phosphate (Dunaway et al., 1988; García et al., 2009) and therefore supports increased glycolysis. Importantly, baseline levels of *Pfk-m* mRNA are higher in *MiR-21*$^{-/-}$ BMDMs, a trend not observed for other PFK isoforms. Conversely, basal levels of *Pfk-m* mRNA are reduced by overexpression of miR-21 in RAW267.4 (Figure 4E), similarly to *Pdcd4* mRNA, supporting the notion that this isoform represents a bona fide miR-21-target. We thus examined protein expression, which miRNAs preferentially regulate (Selbach et al., 2008), and found that miR-21

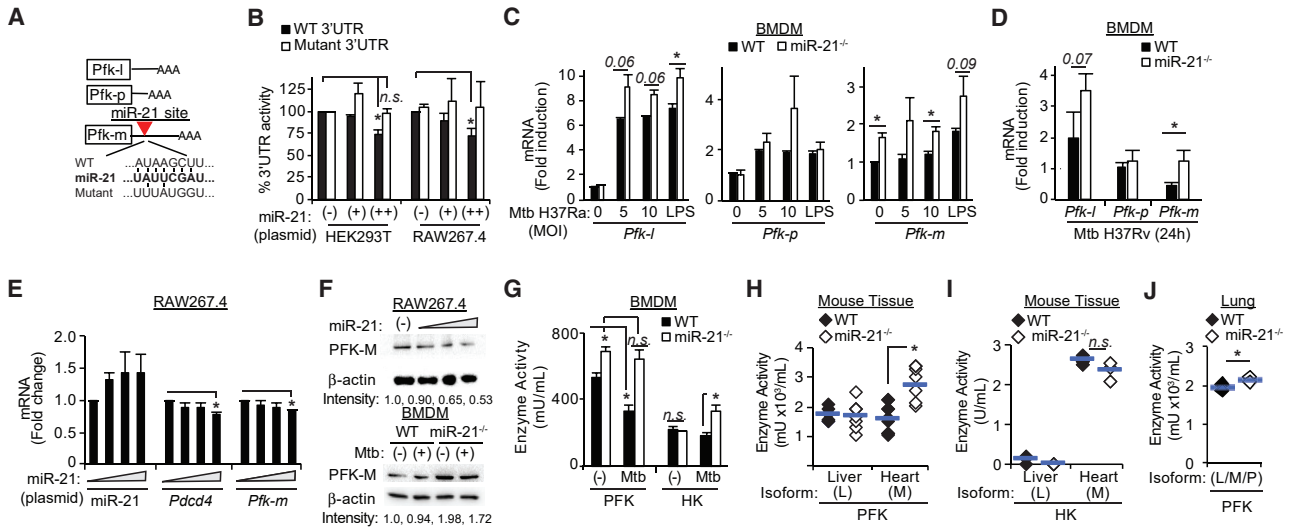

Figure 4. miR-21 Targets the Expression of the Glycolytic Enzyme PFK-M

(A) Schematic of PFK mRNAs indicating the miR-21 site and mutant constructs.

(B) 3′ UTR luciferase reporter activity of PFK-M 3′ UTR (WT 3′ UTR) or mutant construct (mutant 3′ UTR) following co-transfection of HEK293T cells (left) or RAW267.4 cells (right) with control plasmid (–) or increasing amounts of miR-21 overexpressing plasmid (pCMV-miR-21, (+) 25 ng per point, (++) 50 ng per point).

(C and D) qPCR of PFK genes in BMDMs infected with Mtb H37Ra at the indicated MOI or treated with LPS (100 ng/mL) for 24 h (C) or Mtb H37Rv (MOI 5, 24 h) (D).

(E) Relative expression of the indicated RNA species in RAW267.4 cells following 48-h transfection with increasing amounts of miR-21-overexpressing plasmid (pCMV-miR-21, 0–75 ng per point).

(F) PFK-M immunoblot in RAW267.4 macrophages transfected with increasing amounts pCMV-miR-21 as in (E) (top panel) or BMDMs (genotype indicated) before or after infection with Mtb H37Ra (MOI 5, 24 h, bottom panel) alongside β-actin expression (loading control).

(G) *In vitro* enzyme activity for PFK or hexokinase (HK) in BMDMs lysates treated as in (F).

(H–J) *In vitro* PFK (H and J) or HK (I) enzyme activity in the indicated tissues from WT & and miR-21$^{-/-}$ mice (20 mg tissue).

Data represent percent inhibition relative to control transfected cells (A), fold-induction relative to uninfected or control transfected cells (C–E), or mean concentration with individual mouse values indicated (G–J). Blots show one experiment representative of n = 3 independent experiments with normalized PFK-M band intensity provided underneath (F). Data represent mean ± SEM for n = 5 (B, C, E, and G) or n = 3 (D) independent experiments or n = 6 (J–I) or n = 3 (J) mice per group (H–J). *p < 0.05; n.s., p > 0.05 for the indicated group comparisons (ANOVA with post hoc Tukey tests).

overexpression dose-dependently reduced basal PFK-M protein levels in RAW267.4 macrophages (Figure 4F). Although PFK-M protein levels are not significantly altered by Mtb infection in WT BMDMs, levels are dramatically increased in both uninfected and infected *MiR-21*$^{-/-}$ BMDMs (Figure 4F). To confirm the elevated expression relates to augmented enzyme activity, we performed *in vitro* PFK activity assays by providing an excess of fructose-6-phosphate to cell lysates and monitoring the production of linked NADH. Uninfected WT BMDMs had modest PFK activity, which is actually decreased by Mtb infection, supporting the notion that during infection, this key enzyme complex is targeted for negative regulation (Figure 4G). This effect of infection was not observed when the earlier hexokinase step in the glycolytic pathway is measured (Figure 4G). When miR-21 is absent, untreated macrophages have significantly higher PFK, but not hexokinase, activity (Figure 4G), which is resistant to Mtb-induced regulation. PFK activity is determined by multiple isoforms with tissue-specific expression (Dunaway et al., 1988) that can also form functional hetero-tetramers. Each isoform (PFK-L, PFK-P, and PFK-M) is expressed in macrophages. To confirm the differences observed in *MiR-21*$^{-/-}$ BMDMs were specifically due to altered PFK-M expression, we measured PFK activity in murine tissues with defined and restricted expression of each isoform. Specifically, we found that although liver tissue (which solely expresses PFK-L) from WT and *MiR-21*$^{-/-}$ mice displayed similar levels of PFK activity, cardiac muscle tissue (which solely expresses PFK-M) had significantly more PFK activity in *MiR-21*$^{-/-}$ mice (Figure 4H), confirming that restriction of PFK-M by miR-21 controls metabolic activity *in vivo*. As before, no differences between genotypes were observed for hexokinase activity when measured *ex vivo* (Figure 4I). Thus, the increased PFK activity measured in miR-21-deficient BMDM is likely due to altered expression of the PFK-M isoform. Lung tissue, the primary site of Mtb infection, expresses all three PFK isoforms (Shi et al., 2015). Despite this, a modest but significant increase in PFK enzyme activity is measured in lungs from *MiR-21*$^{-/-}$ animals (Figure 4J), suggesting that miR-21 plays a role limiting glycolysis in this environment during the immune response.

Targeting of PFK-M by miR-21 Controls Mtb Responses

Since our results suggested an important role for PFK-M regulating glycolysis during Mtb infection that impacts host defense, we more directly targeted *Pfk-m* itself using small interfering RNA (siRNA). Although knockdown was not observed in uninfected BMDMs, which express low basal levels of PFK-M protein, our siRNA transfection led to knockdown after treatment with hk-Mtb, which normally stabilizes PFK-M protein expression and

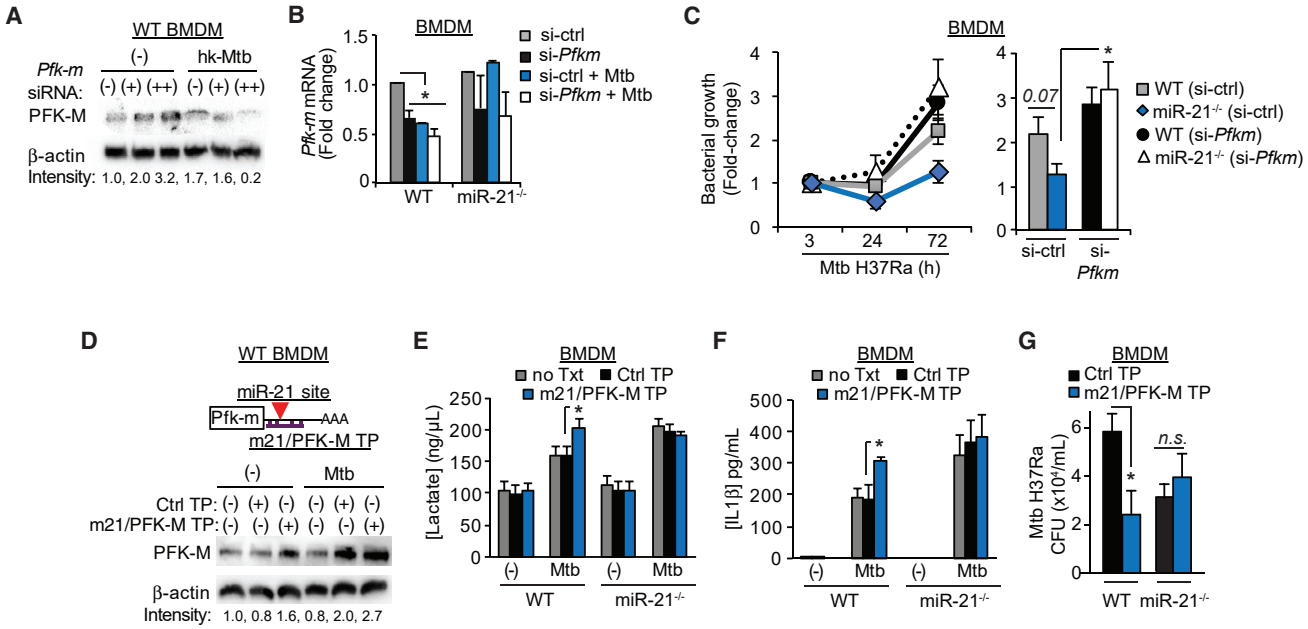

Figure 5. Targeting of PFK-M by miR-21 Controls Mtb Responses

(A) PFK-M immunoblot in BMDMs transfected with increasing amounts of *Pfk-m*-specific siRNA (25 nM (+), 50 nM (++)) or control non-targeting siRNA (–), treated with hk-Mtb (MOI 5, 24 h) alongside β-actin expression (loading control).

(B) qPCR of *Pfk-m* mRNA in BMDMs (genotype indicated) transfected with 50 nM *Pfk-m*-specific (si-*Pfk-m*) or control non-targeting (si-Ctrl) siRNA and subsequently infected with Mtb H37Ra (MOI 5, 24 h).

(C) Bacterial growth in BMDMs treated as (B) for up to 72 h.

(D) Target protection schematic showing PFK-m 3′ UTR and miR-21/PFK-M-specific morpholino (m21/PFK-M TP, top) and PFK-M immunoblot of BMDMs transfected with 10 μM control non-targeting morpholino (Ctrl TP) or m21/PFK-m TP or empty transfected cells (–) and subsequently infected with Mtb H37Ra (MOI 5, 24 h) or β-actin expression (loading control).

(E and F) Lactate production (E) or IL-1β ELISA (F) in supernatants from BMDMs transfected with 10 μM non-targeting morpholino (Ctrl TP) or m21/PFKm TP or empty transfected cells (no Txt) and infected with Mtb H37Ra (Mtb; MOI 5, 24 h).

(G) Bacterial CFUs of BMDMs treated as in (E) for up to 72 h.

Blots show one experiment representative of n = 2 (A) or n = 3 independent experiments (D). mRNA data represent fold-induction relative to uninfected si-Ctrl transfected WT BMDMs (B). Bacterial growth is presented as fold-change in baseline CFUs (3 h; C) or CFU values at 72 h. Lactate and ELISA data represent mean concentration (E and F). All data represent mean ± SEM of n = 3 independent experiments. *p < 0.05; n.s., p > 0.05 for the indicated group comparisons (ANOVA with post hoc Tukey tests).

drives glycolysis (Figure 5A). Importantly, the induction of glycolysis after hk-Mtb treatment was significantly impaired by PFK-M knockdown, as was the production of IL-1β (Figures S6E and S6F). During infection of BMDMs with live Mtb H37Ra, we measured knockdown using qPCR and found significant reduction in basal *Pfk-m* mRNA levels (up to 50%; Figure 5B), an effect mirrored by infection with Mtb H37Ra. Importantly, whereas the decrease in *Pfk-m* mRNA by Mtb infection is normally impaired in *MiR-21*$^{-/-}$ BMDMs, siRNA transfection maintained this at low levels (Figure 5B), allowing us to specifically examine the role of *Pfk-m* targeting my miR-21. The enhanced ability of *MiR-21*$^{-/-}$ BMDMs to contain Mtb intracellular growth is lost when increased PFK-M expression is targeted by siRNA (Figure 5C), confirming the importance if this molecule controlling the immunometabolic response to Mtb.

To confirm directly that this repression impacts Mtb responses, we employed a target protection strategy (Choi et al., 2007) to specifically block the interaction of *Pfk-m* mRNA and miR-21 (Figure 5D). Transfection of WT BMDMs with this oligonucleotide increased PFK-M protein levels in both uninfected and Mtb-infected macrophages (Figure 5D). Similarly, extracellular levels of lactate and IL-1β were enhanced (Figures 5E and 5F), as was the ability to contain intracellular Mtb (Figure 5G). Importantly, these effects are phenocopied, but not enhanced, by oligonucleotide treatment in *MiR-21*$^{-/-}$ BMDMs. Target protection does not alter the changes observed in Mtb-induced TNF or IL-10 production across genotypes (Figures S6G and S6H). Collectively, these data support the notion that Mtb targets this key step in the glycolytic pathway to limit host responses via persistent upregulation of miR-21, which inhibits the expression of the pro-glycolytic PFK-M isoenzyme and subsequent activation of host defense through IL-1β production.

miR-21 Impacts AM Immunometabolic Responses to Mtb

After confirming the importance of the miR-21/PFK-M axis in the model mouse BMDM and hMDM systems, which mimic macrophages recruited to sites of infection, we investigated the primary host cell for Mtb, the resident alveolar macrophage

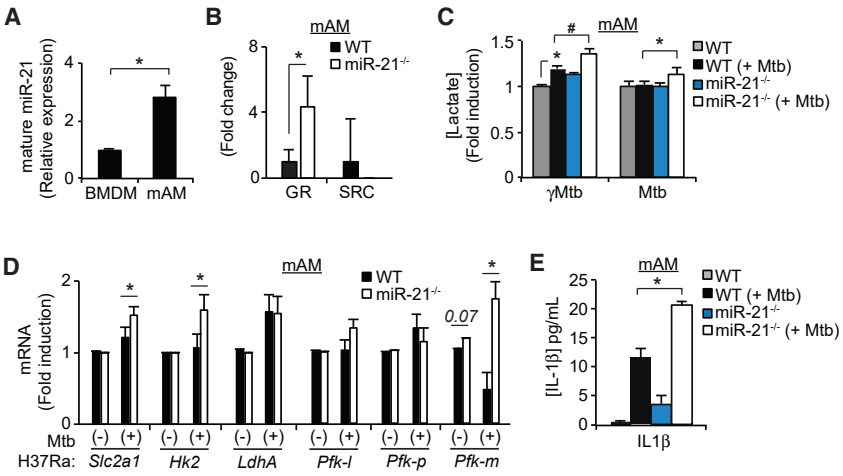

Figure 6. miR-21 Limits Alveolar Macrophage Responses to Mtb Infection

(A) qPCR of mature miR-21 in resting BMDMs or mouse alveolar macrophages (mAMs).

(B) GR and SRC of resting BMDMs or mAMs (genotype indicated).

(C) Extracellular lactate from mAMs (genotype indicated) treated with γ-irradiated Mtb (γMtb) or infected with Mtb H37Ra (Mtb; MOI 5, 24 h).

(D) qPCR of indicated genes in mAMs (genotype indicated) infected with Mtb H37Ra (MOI 5, 24 h).

(E) IL-1β ELISA in supernatants from mAMs treated as in (D).

Data represent normalized ΔCt values across cell types (A), fold change in indicated parameter relative to WT mAMs (B), mean fold-change in lactate production relative to uninfected WT mAMs (C), fold induction relative to uninfected WT mAMs (D), and mean concentration (E). All experiments are mean ± SEM for n = 3 mice per group. *p < 0.05 and #p < 0.05 for the indicated group comparisons (ANOVA with post hoc Tukey tests in C–E or Student's t test in A and B).

(AM), which we and others recently described as having metabolic plasticity dependent on both ontogeny and local environmental signals (Gleeson et al., 2018; Huang et al., 2018). First, we compared basal levels of mature miR-21 in mouse AMs (mAMs) or mature BMDMs and found strikingly higher levels of miR-21 in mAMs (Figure 6A), also seen in hAMs versus hMDMs (Figure S7A). AMs possess distinct metabolic properties from BMDMs and induce less glycolysis after infection; therefore, we measured maximal glycolytic capacity and found that mAMs from *MiR-21*$^{-/-}$ mice have an increased GR compared to their WT counterparts, more akin to BMDMs, with no effect on SRC (Figure 6B). Stimulation with γMtb induced modest extracellular lactate accumulation, which was enhanced in the absence of miR-21 (Figure 6C). Infection with live Mtb H37Ra did not lead to a similar boost in lactate production in WT mAMs, consistent with high levels of miR-21 and low glycolytic potential. However, although low, lactate induction was significantly enhanced in *MiR-21*$^{-/-}$ AMs (Figure 6C), supporting the notion that the presence of miR-21 exerts a limiting effect on the glycolytic potential of these cells. Little to no significant induction of *Slc2a1*, *Hk2*, or *LdhA* mRNAs was observed in WT mAMs after infection with viable Mtb H37Ra (Figure 6D), unlike that seen in BMDMs (Figure 2D). However, more *Slc2a1* and *Hk2* mRNA induction was observed in *MiR-21*$^{-/-}$ mAMs (Figure 6D). We observed a trend toward basally higher *Pfk-m* mRNA (p = 0.07) in *MiR-21*$^{-/-}$ mAMs than in WT, and while infection with Mtb H37Ra decreased *Pfk-m* mRNA levels in WT mAMs, this was stabilized and actually increased in *MiR-21*$^{-/-}$ mAMs (Figure 6D). With respect to host responses, there was significantly more accumulation of IL-1β protein in supernatants from Mtb-infected *MiR-21*$^{-/-}$ AMs (Figure 6E). A similar enhancement of *IL1B* mRNA was seen in hAMs transfected with miR-21 antisense prior to activation with LPS (Figure S7B). These results highlight the importance of miR-21 expression regulating the metabolic plasticity and immune phenotype of resident macrophages, which is influenced by both ontogeny and the nature of activating stimuli encountered during infection.

Activation of Macrophages by IFN-γ Targets Glycolysis via miR-21

We wondered whether other signals involved in the immune response could impact on the immunometabolic pathway via miR-21. Increased glycolysis has emerged as a cardinal feature of "M1" macrophages, which have been treated *in vitro* with a Toll-like receptor (TLR) ligand (LPS) and IFN-γ (Jha et al., 2015). In fact, IFN-γ treatment of LPS-activated BMDMs specifically enhances rates of glycolysis (Figure 7A) and lactate production in Mtb-infected BMDMs (Figure 7B) and hMDMs (Figure S7C). Increased glycolysis is required for the potentiation of TLR-related genes, including *Il1b* by IFN-γ, since growing hMDMs in galactose-containing media reduces the boost in IL-1β production by IFN-γ (Figure 7C). IFN-γ also supports enhanced induction of glycolytic genes (*Slc2a1*, *Hk2*, and *Ldha*; Figure 7D) during Mtb infection. Interestingly, the boost in IL-1β expression by IFN-γ is not apparent in miR-21-silenced MDMs (Figure 7C) or *MiR-21*$^{-/-}$ BMDMs (Figure S7D). Intriguingly, the IFN-γ-mediated boost in lactate production in WT BMDMs reaches levels similar to that seen in miR-21-deficient cells (Figures 7B and S7C), suggesting that IFN-γ overcomes miR-21 repression of glycolysis to promote its pro-inflammatory and anti-microbial activities. We therefore examined miR-21 levels in IFN-γ-treated cells. Although IFN-γ alters transcription of target genes (Hu and Ivashkiv, 2009), we did not observe alterations in *pri-miR-21* transcript levels in IFN-γ-primed BMDMs after 24-h LPS treatment or infection with Mtb H37Ra (Figure 7E). However, a decrease was noted in the levels of the mature miR-21 species after IFN-γ treatment (Figure 7E). These data suggest that IFN-γ targets miR-21 production to temper its anti-inflammatory effects and negative regulation of glycolysis. Accordingly, *Pfk-m* mRNA, which normally decreases after Mtb infection, is maintained by IFN-γ (Figure 7E), with an increase in PFK-M protein expression in IFN-γ-primed BMDMs (Figure 7F). This corresponds with an ~20% increase in PFK activity in Mtb-infected cells following IFN-γ priming, which is not observed in *MiR-21*$^{-/-}$ BMDMs or at the level of hexokinase activity (Figure 7G), suggesting that IFN-γ counteracts the

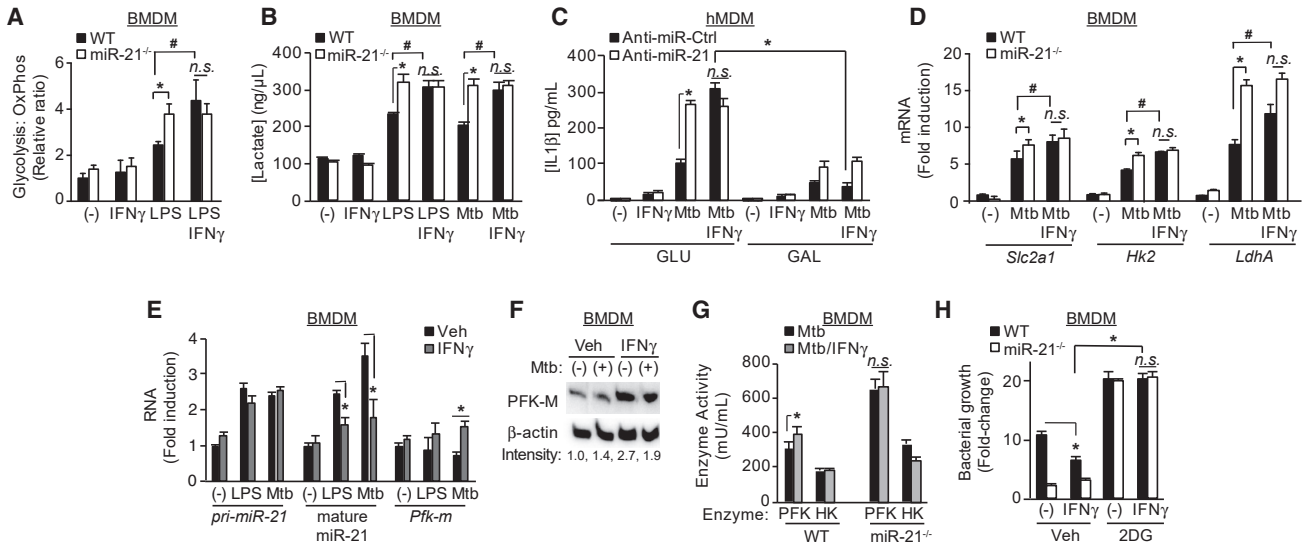

Figure 7. Activation of Macrophages by IFN-γ Targets Glycolysis via miR-21

(A) ECAR:OCR ratio in BMDMs (genotype indicated) primed with IFNγ (5 ng/mL) before treatment with LPS (100 ng/mL).

(B) Extracellular lactate from BMDMs (genotype indicated) primed with IFN-γ (5 ng/mL) before treatment with LPS (100 ng/mL) or infection with Mtb H37Ra (MOI 5, 24 h).

(C) IL-1β ELISA in supernatants from hMDMs transfected with 50 nM miR-21-specific antisense (anti-miR-21) or a control nonspecific antisense (anti-miR-Ctrl) 24 h prior to treatment with IFN-γ (5 ng/mL) and/or infection with Mtb H37Ra (MOI 5, 24 h) in glucose-containing media (GLU) or glucose-free galactose-containing media (GAL).

(D) qPCR of indicated genes in BMDMs (genotype indicated) primed with IFN-γ (5 ng/mL) before infection with Mtb H37Ra (MOI 5, 24 h).

(E) qPCR of indicated RNA species in BMDMs primed with IFN-γ (5 ng/mL) before treatment with LPS (100 ng/mL) or infection with Mtb H37Ra (MOI 5) for 24 h.

(F) PFK-M immunoblot of BMDMs treated as in (E).

(G) In-vitro enzyme activity for phosphofructokinase (PFK) or hexokinase (HK) in lysates from BMDM treated as in D.

(H) Bacterial growth in BMDMs (genotype indicated) primed with IFN-γ (5 ng/mL) before infection with Mtb H37Ra (MOI 5, 72 h) with treatment with 10 mM 2DG or vehicle 3 h post-infection.

Data represent mean fold-change over uninfected (A, D, E, and H) or mean concentration (B, C, and G). Data represent mean ± SEM of n = 3 independent experiments (A–E and H) with one blot representative of n = 3 (F) or mean activity ± SEM for n = 6 (PFK) or n = 5 (HK) independent experiments (G). *p < 0.05 and #p < 0.05 for the indicated group comparisons (ANOVA with post hoc Tukey tests).

inhibitory effects of Mtb by buffering the increase in miR-21. Since IFN-γ plays an important role in tuberculosis (TB) host defense (Bogunovic et al., 2012), we wondered if its anti-microbial effects proceeded through the miR-21/glycolysis axis. Again, IFN-γ treatment, which improves the ability of macrophages to contain Mtb, is phenocopied by *MiR-21*$^{-/-}$ BMDMs (Figure 7H). This antimicrobial effect of IFN-γ requires glycolysis, since it is blocked in both WT and *MiR-21*$^{-/-}$ BMDMs by 2DG, which permits mycobacterial growth despite the presence of IFN-γ (Figure 7H). This places miR-21 expression as an important molecular switch that balances the immunometabolic response of macrophages, targeted by both pathogen and host-encoded processes to shape immunity.

DISCUSSION

By examining how Mtb manipulates innate immunity, we have identified a central regulator of the macrophage immunometabolic response: control of PFK-M expression, activity, and glycolysis by a miRNA, miR-21. Whereas miR-21 was previously shown to negatively regulate innate immunity by modulating both pro- and anti-inflammatory cytokine production (Barnett et al., 2016; Chen et al., 2013; Das et al., 2014; Liu et al., 2012; Lu et al., 2011; Merline et al., 2011; Sheedy et al., 2010), the engagement of a novel mRNA target by miR-21 in the context of Mtb infection points toward the importance of the immunometabolic response in host defense and expands the identified targets for miR-21 that regulate innate immunity.

It is now apparent that the nutrients utilized by and the metabolic pathways engaged determine immune cell function, but these can be manipulated by environmental signals, both activating and inhibitory (Hobson-Gutierrez and Carmona-Fontaine, 2018). While activation of macrophages by microbial-sensing TLRs, particularly TLR4, is known to subvert TCA (Jha et al., 2015) and lead to increased reliance on glycolysis driven by HIF-1α (Rodríguez-Prados et al., 2010; Tannahill et al., 2013), less is known about the molecular mechanisms regulating this over time and during infection. We recently described the switch to increased glycolysis, critical for the ability of macrophages to contain Mtb, early in infection (Gleeson et al., 2016). Here, we demonstrate that this is temporally regulated during infection, with blunting of this process apparent in macrophages infected with proliferating mycobacteria. Furthermore, we show that augmenting production of mature miR-21 levels is central to mediating this control, suggesting that during infection, Mtb manipulates an endogenous host mechanism for the resolution of

inflammation (Das et al., 2014) to co-opt macrophage function and maintain an environment favorable to bacillary replication.

Central to this is the production of IL-1β, which we and others have recently shown is critical in macrophage containment of Mtb (Gleeson et al., 2016; Mayer-Barber et al., 2014). Though IL-1β production is controlled at multiple levels (Próchnicki and Latz, 2017), in recent years, it has been appreciated that later potentiation of its transcription occurs through HIF-1α (Tannahill et al., 2013), driven by increased glycolysis (Palsson-McDermott et al., 2015). Our work with Mtb, which drives both transcriptional induction and inflammasome activation (Mishra et al., 2010), revealed that miR-21 impacts IL-1β transcription, a finding not previously observed but upheld following induction of *Il1b* by the TLR4 ligand LPS. Even though miR-21 has been linked to negative regulation of pro-inflammatory processes, including TNF production (Das et al., 2014; Liu et al., 2012) and promotion of anti-inflammatory responses like IL-10 (Das et al., 2014; Merline et al., 2011; Sheedy et al., 2010), these data place IL-1β as a key cytokine sensitive to regulation by miR-21 and are consistent with recent data from studies of leprosy (Liu et al., 2012). Although it has been suggested that *Il1b* mRNA is a direct target for repression by miR-21 (Liu et al., 2012; Terao et al., 2011), our data demonstrate indirect transcriptional regulation through modulating macrophage metabolism. Recently, multi-drug-resistant strains of Mtb were shown to limit IL-1β production through reduced metabolic reprogramming (Howard et al., 2018). Although we use both attenuated (H37Ra) and virulent (H37Rv) lab Mtb strains for functional studies, in both cases, negative regulation of glycolysis and pro-inflammatory signaling by miR-21 was observed. It may be the case that more clinically relevant and drug-resistant strains, which differentially modulate cytokine production, may in fact mediate these effects through miR-21 induction, and this remains to be tested.

Our studies of miR-21-deficient cells revealed unregulated glycolysis, despite intact glucose-fueled TCA basally. When interrogated Mtb did reduce SRC, which is consistent with an increased reliance on glycolysis and findings that Mtb infection of macrophages blocks fatty-acid oxidation to mobilize intracellular lipids (Knight et al., 2018; Ouimet et al., 2016; Russell et al., 2009). Therefore, it is clear that the reprogramming of central energy metabolism observed during Mtb infection is distinct from the traditional "Warburg effect" observed in LPS-stimulated macrophages or tumor cells (Koppenol et al., 2011), with increased glycolytic rates being a key feature of infected macrophages. We show that this is limited over time by targeting the expression of a pro-glycolytic isoenzyme of the rate-limiting PFK-1 step of glycolysis (Dunaway et al., 1988; García et al., 2009; Tanner et al., 2018), which restricts flux through the glycolytic pathway and subsequent lactate production. These results are supported by a recent study that noted decreased glycolysis and lactate accumulation in Mtb-infected macrophages and, through metabolic flux analysis of glycolytic intermediates, pointed toward regulation at the level of PFK (Cumming et al., 2018). Increased metabolism of glucose through glycolysis has been suggested to promote macrophage activation by providing a rapid source of ATP and increasing levels of biosynthetic precursors required for inflammatory responses. Intermediates of nucleotides, amino acids, and lipids accumulate by feeding anabolic pathways from glycolysis, including the pentose-phosphate pathway (PPP). Crucially, the decision to commit to this pathway is regulated by PFK activity, and a decrease in pro-glycolytic PFK-M by Mtb-induced miR-21 may in fact support an alternative fate for carbon intermediates feeding into the PPP. Our observation that glucose consumption in WT and miR-21-deficent macrophages after infection remains unaltered, despite their ability to produce increased levels of lactate and increased PFK activity, suggests a complex reprogramming of kinetics and nutrient utilization that is central to host-pathogen interactions. Targeting glycolysis at PFK-1 could allow bacteria to bypass host pro-inflammatory events fueled by increased glycolysis (Braverman and Stanley, 2017; Garaude et al., 2016; Gleeson et al., 2016; Palsson-McDermott et al., 2015) yet support immune evasion associated with altering intracellular anabolic pathways such as the PPP (Ouimet et al., 2016), including fatty acid synthesis or nucleotide production required for bacterial replication.

PFK-1 activity is also modulated by the host cytokine, IFN-γ, during Mtb infection. By relieving the repression of PFK-M by specifically modulating mature miR-21, IFN-γ can reprogram cellular metabolism to support pro-inflammatory activities. Consistent with this, IFN-γ-driven HIF-1α and nitric oxide (NO) production have emerged as key processes sensitive to changes in glycolysis (Braverman et al., 2016; Braverman and Stanley, 2017) that miR-21 also impact. Reprogramming of macrophage protein production by mTOR has been shown to be critical in IFN-γ signaling (Su et al., 2015) and is mediated in part through modulation of miRNA levels. The specific negative regulation of the mature miR-21 species by IFN-γ implies post-transcriptional regulation, which was previously observed for miR-21 during transforming growth factor β (TGF-β) signaling mediated through SMAD proteins (Su et al., 2015), which are also targets in IFN-γ signaling (Ghosh et al., 2001). This results in increased PFK-M expression and subsequent glycolytic flux in activated macrophages, facilitating pro-inflammatory signaling. Apart from increased glycolytic flux, how altered metabolic activities and intermediates downstream of increased PFK-1 activity contribute to the pro-inflammatory and antimicrobial effects of IFN-γ remain unclear. Recent studies suggest the mobilization of lipids in Mtb-infected cells contribute to IFN-γ activity (Knight et al., 2018), and the targeting of miR-21 observed here could contribute to this by driving flux through glycolysis to promote glyceraldehyde 3-phosphate production. Novel anti-mycobacterial strategies promoting IFN-γ activity are being developed, and our work suggests these may proceed by modulating miRNA expression. Since recent work suggests that the metabolic activity of resident cells contributes to pulmonary compartment susceptibility to TB (Gleeson et al., 2018; Huang et al., 2018), a better understanding of the signals and mechanisms that underline this immunometabolic response, like our identification of a novel mRNA target and cellular process engaged by miR-21, provides a rationale for boosting defective immunity in chronic infection like tuberculosis and also other pulmonary diseases and cancer, where control of metabolic flux can have diverse and specific effects (Hobson-Gutierrez and Carmona-Fontaine, 2018).

STAR★METHODS

Detailed methods are provided in the online version of this paper and include the following:

- KEY RESOURCES TABLE
- LEAD CONTACT AND MATERIALS AVAILABILITY
- EXPERIMENTAL MODEL AND SUBJECT DETAILS
  - Animals
  - Cell isolation and culture
  - Mycobacterium tuberculosis infections
- METHOD DETAILS
  - Gene Expression analysis
  - Metabolic assays
  - ELISA, Cell Viability, Nitrite and Intracellular ROS Assays
  - Transfection and Plasmids
- QUANTIFICATION AND STATISTICAL ANALYSIS
- DATA AND CODE AVAILABILITY

SUPPLEMENTAL INFORMATION

Supplemental Information can be found online at https://doi.org/10.1016/j.celrep.2019.12.015.

ACKNOWLEDGMENTS

Support for this work came from Science Foundation Ireland (starting investigator grants SFI/SIRG/2136 to F.J.S., 11/SIRG/B2099 to S.C.C., 12/1A/1421 to E.C.L. and 15/IA/3154 to S.V.G.), the Health Research Board, Ireland (CSA/2012/16), the Royal City of Dublin Hospital Trust (J.K.), and Irish Research Council (GOIPG/2017/1954 to S.C.. and GOIPD/2019/807 to H.C.-M.) and National Institutes Of Health R35 HL135799 to K.J.M.

AUTHOR CONTRIBUTIONS

E.E.H. and H.C.-M. performed and analyzed all experiments. S.M.O., L.E.G., A.S., and S.V.G. provided assistance with Mtb infections. N.M.-W., D.G.J., M.W., S.C., A.W., E.C.L., and S.C.C. provided assistance with miR-21-deficient animals. M.O. and K.J.M. performed the experiments shown in Figure 1K. J.K. conceived ideas and co-supervised the work. F.J.S. performed experiments, performed analysis, supervised the work, and wrote the paper.

DECLARATION OF INTERESTS

The authors declare no competing interests.

Received: April 24, 2019
Revised: November 6, 2019
Accepted: December 5, 2019
Published: January 7, 2020

REFERENCES

Barnett, R.E., Conklin, D.J., Ryan, L., Keskey, R.C., Ramjee, V., Sepulveda, E.A., Srivastava, S., Bhatnagar, A., and Cheadle, W.G. (2016). Anti-inflammatory effects of miR-21 in the macrophage response to peritonitis. J. Leukoc. Biol. *99*, 361–371.

Bogunovic, D., Byun, M., Durfee, L.A., Abhyankar, A., Sanal, O., Mansouri, D., Salem, S., Radovanovic, I., Grant, A.V., Adimi, P., et al. (2012). Mycobacterial disease and impaired IFN-γ immunity in humans with inherited ISG15 deficiency. Science *337*, 1684–1688.

Braverman, J., and Stanley, S.A. (2017). Nitric oxide modulates macrophage responses to *Mycobacterium tuberculosis* infection through activation of HIF-1α and repression of NF-κB. J. Immunol. *199*, 1805–1816.

Braverman, J., Sogi, K.M., Benjamin, D., Nomura, D.K., and Stanley, S.A. (2016). HIF-1α Is an Essential Mediator of IFN-γ-Dependent Immunity to Mycobacterium tuberculosis. J. Immunol. *197*, 1287–1297.

Chen, Y., Chen, J., Wang, H., Shi, J., Wu, K., Liu, S., Liu, Y., and Wu, J. (2013). HCV-induced miR-21 contributes to evasion of host immune system by targeting MyD88 and IRAK1. PLoS Pathog. *9*, e1003248.

Choi, W.Y., Giraldez, A.J., and Schier, A.F. (2007). Target protectors reveal dampening and balancing of Nodal agonist and antagonist by miR-430. Science *318*, 271–274.

Cumming, B.M., Addicott, K.W., Adamson, J.H., and Steyn, A.J. (2018). *Mycobacterium tuberculosis* induces decelerated bioenergetic metabolism in human macrophages. eLife *7*, e39169.

Das, A., Ganesh, K., Khanna, S., Sen, C.K., and Roy, S. (2014). Engulfment of apoptotic cells by macrophages: a role of microRNA-21 in the resolution of wound inflammation. J. Immunol. *192*, 1120–1129.

Dunaway, G.A., Kasten, T.P., Sebo, T., and Trapp, R. (1988). Analysis of the phosphofructokinase subunits and isoenzymes in human tissues. Biochem. J. *251*, 677–683.

Everts, B., Amiel, E., Huang, S.C., Smith, A.M., Chang, C.H., Lam, W.Y., Redmann, V., Freitas, T.C., Blagih, J., van der Windt, G.J., et al. (2014). TLR-driven early glycolytic reprogramming via the kinases TBK1-IKKε supports the anabolic demands of dendritic cell activation. Nat. Immunol. *15*, 323–332.

Flynn, J.L., Goldstein, M.M., Chan, J., Triebold, K.J., Pfeffer, K., Lowenstein, C.J., Schreiber, R., Mak, T.W., and Bloom, B.R. (1995). Tumor necrosis factor-alpha is required in the protective immune response against Mycobacterium tuberculosis in mice. Immunity *2*, 561–572.

Garaude, J., Acín-Pérez, R., Martínez-Cano, S., Enamorado, M., Ugolini, M., Nistal-Villán, E., Hervás-Stubbs, S., Pelegrín, P., Sander, L.E., Enríquez, J.A., and Sancho, D. (2016). Mitochondrial respiratory-chain adaptations in macrophages contribute to antibacterial host defense. Nat. Immunol. *17*, 1037–1045.

García, M., Pujol, A., Ruzo, A., Riu, E., Ruberte, J., Arbós, A., Serafín, A., Albella, B., Felíu, J.E., and Bosch, F. (2009). Phosphofructo-1-kinase deficiency leads to a severe cardiac and hematological disorder in addition to skeletal muscle glycogenosis. PLoS Genet. *5*, e1000615.

Ghosh, A.K., Yuan, W., Mori, Y., Chen Sj, and Varga, J. (2001). Antagonistic regulation of type I collagen gene expression by interferon-gamma and transforming growth factor-beta. Integration at the level of p300/CBP transcriptional coactivators. J. Biol. Chem. *276*, 11041–11048.

Gleeson, L.E., Sheedy, F.J., Palsson-McDermott, E.M., Triglia, D., O'Leary, S.M., O'Sullivan, M.P., O'Neill, L.A., and Keane, J. (2016). Cutting Edge: Mycobacterium tuberculosis induces aerobic glycolysis in human alveolar macrophages that is required for control of intracellular bacillary replication. J. Immunol. *196*, 2444–2449.

Gleeson, L.E., O'Leary, S.M., Ryan, D., McLaughlin, A.M., Sheedy, F.J., and Keane, J. (2018). Cigarette smoking impairs the bioenergetic immune response to Mycobacterium tuberculosis infection. Am. J. Respir. Cell Mol. Biol. *59*, 572–579.

Gohil, V.M., Sheth, S.A., Nilsson, R., Wojtovich, A.P., Lee, J.H., Perocchi, F., Chen, W., Clish, C.B., Ayata, C., Brookes, P.S., and Mootha, V.K. (2010). Nutrient-sensitized screening for drugs that shift energy metabolism from mitochondrial respiration to glycolysis. Nat. Biotechnol. *28*, 249–255.

Graff, J.W., Dickson, A.M., Clay, G., McCaffrey, A.P., and Wilson, M.E. (2012). Identifying functional microRNAs in macrophages with polarized phenotypes. J. Biol. Chem. *287*, 21816–21825.

Hobson-Gutierrez, S.A., and Carmona-Fontaine, C. (2018). The metabolic axis of macrophage and immune cell polarization. Dis. Model. Mech. *11*, dmm034462.

Howard, N.C., Marin, N.D., Ahmed, M., Rosa, B.A., Martin, J., Bambouskova, M., Sergushichev, A., Loginicheva, E., Kurepina, N., Rangel-Moreno, J., et al. (2018). Mycobacterium tuberculosis carrying a rifampicin drug resistance

mutation reprograms macrophage metabolism through cell wall lipid changes. Nat. Microbiol. *3*, 1099–1108.

Hu, X., and Ivashkiv, L.B. (2009). Cross-regulation of signaling pathways by interferon-gamma: implications for immune responses and autoimmune diseases. Immunity *31*, 539–550.

Huang, L., Nazarova, E.V., Tan, S., Liu, Y., and Russell, D.G. (2018). Growth of *Mycobacterium tuberculosis* in vivo segregates with host macrophage metabolism and ontogeny. J. Exp. Med. *215*, 1135–1152.

Ip, W.K.E., Hoshi, N., Shouval, D.S., Snapper, S., and Medzhitov, R. (2017). Anti-inflammatory effect of IL-10 mediated by metabolic reprogramming of macrophages. Science *356*, 513–519.

Jha, A.K., Huang, S.C., Sergushichev, A., Lampropoulou, V., Ivanova, Y., Loginicheva, E., Chmielewski, K., Stewart, K.M., Ashall, J., Everts, B., et al. (2015). Network integration of parallel metabolic and transcriptional data reveals metabolic modules that regulate macrophage polarization. Immunity *42*, 419–430.

Johnston, D.G.W., Kearney, J., Zasłona, Z., Williams, M.A., O'Neill, L.A.J., and Corr, S.C. (2017). MicroRNA-21 Limits Uptake of *Listeria monocytogenes* by Macrophages to Reduce the Intracellular Niche and Control Infection. Front. Cell. Infect. Microbiol. *7*, 201.

Knight, M., Braverman, J., Asfaha, K., Gronert, K., and Stanley, S. (2018). Lipid droplet formation in Mycobacterium tuberculosis infected macrophages requires IFN-γ/HIF-1α signaling and supports host defense. PLoS Pathog. *14*, e1006874.

Koppenol, W.H., Bounds, P.L., and Dang, C.V. (2011). Otto Warburg's contributions to current concepts of cancer metabolism. Nat. Rev. Cancer *11*, 325–337.

Kumar, R., Halder, P., Sahu, S.K., Kumar, M., Kumari, M., Jana, K., Ghosh, Z., Sharma, P., Kundu, M., and Basu, J. (2012). Identification of a novel role of ESAT-6-dependent miR-155 induction during infection of macrophages with Mycobacterium tuberculosis. Cell. Microbiol. *14*, 1620–1631.

Lachmandas, E., Beigier-Bompadre, M., Cheng, S.C., Kumar, V., van Laarhoven, A., Wang, X., Ammerdorffer, A., Boutens, L., de Jong, D., Kanneganti, T.D., et al. (2016a). Rewiring cellular metabolism via the AKT/mTOR pathway contributes to host defence against Mycobacterium tuberculosis in human and murine cells. Eur. J. Immunol. *46*, 2574–2586.

Lachmandas, E., Boutens, L., Ratter, J.M., Hijmans, A., Hooiveld, G.J., Joosten, L.A., Rodenburg, R.J., Fransen, J.A., Houtkooper, R.H., van Crevel, R., et al. (2016b). Microbial stimulation of different Toll-like receptor signalling pathways induces diverse metabolic programmes in human monocytes. Nat. Microbiol. *2*, 16246.

Liu, P.T., Wheelwright, M., Teles, R., Komisopoulou, E., Edfeldt, K., Ferguson, B., Mehta, M.D., Vazirnia, A., Rea, T.H., Sarno, E.N., et al. (2012). MicroRNA-21 targets the vitamin D-dependent antimicrobial pathway in leprosy. Nat. Med. *18*, 267–273.

Lu, T.X., Hartner, J., Lim, E.J., Fabry, V., Mingler, M.K., Cole, E.T., Orkin, S.H., Aronow, B.J., and Rothenberg, M.E. (2011). MicroRNA-21 limits in vivo immune response-mediated activation of the IL-12/IFN-gamma pathway, Th1 polarization, and the severity of delayed-type hypersensitivity. J. Immunol. *187*, 3362–3373.

Martin, B., Hirota, K., Cua, D.J., Stockinger, B., and Veldhoen, M. (2009). Interleukin-17-producing gammadelta T cells selectively expand in response to pathogen products and environmental signals. Immunity *31*, 321–330.

Mayer-Barber, K.D., Andrade, B.B., Oland, S.D., Amaral, E.P., Barber, D.L., Gonzales, J., Derrick, S.C., Shi, R., Kumar, N.P., Wei, W., et al. (2014). Host-directed therapy of tuberculosis based on interleukin-1 and type I interferon crosstalk. Nature *511*, 99–103.

Merline, R., Moreth, K., Beckmann, J., Nastase, M.V., Zeng-Brouwers, J., Tralhão, J.G., Lemarchand, P., Pfeilschifter, J., Schaefer, R.M., Iozzo, R.V., and Schaefer, L. (2011). Signaling by the matrix proteoglycan decorin controls inflammation and cancer through PDCD4 and MicroRNA-21. Sci. Signal. *4*, ra75.

Mishra, B.B., Moura-Alves, P., Sonawane, A., Hacohen, N., Griffiths, G., Moita, L.F., and Anes, E. (2010). Mycobacterium tuberculosis protein ESAT-6 is a potent activator of the NLRP3/ASC inflammasome. Cell. Microbiol. *12*, 1046–1063.

Mor, I., Cheung, E.C., and Vousden, K.H. (2011). Control of glycolysis through regulation of PFK1: old friends and recent additions. Cold Spring Harb. Symp. Quant. Biol. *76*, 211–216.

O'Garra, A., Redford, P.S., McNab, F.W., Bloom, C.I., Wilkinson, R.J., and Berry, M.P. (2013). The immune response in tuberculosis. Annu. Rev. Immunol. *31*, 475–527.

Ouimet, M., Koster, S., Sakowski, E., Ramkhelawon, B., van Solingen, C., Oldebeken, S., Karunakaran, D., Portal-Celhay, C., Sheedy, F.J., Ray, T.D., et al. (2016). Mycobacterium tuberculosis induces the miR-33 locus to reprogram autophagy and host lipid metabolism. Nat. Immunol. *17*, 677–686.

Palsson-McDermott, E.M., Curtis, A.M., Goel, G., Lauterbach, M.A., Sheedy, F.J., Gleeson, L.E., van den Bosch, M.W., Quinn, S.R., Domingo-Fernandez, R., Johnston, D.G., et al. (2015). Pyruvate kinase M2 regulates Hif-1α activity and IL-1β induction and is a critical determinant of the warburg effect in LPS-activated macrophages. Cell Metab. *21*, 65–80.

Pearce, E.L., and Pearce, E.J. (2013). Metabolic pathways in immune cell activation and quiescence. Immunity *38*, 633–643.

Pitt, J.M., Stavropoulos, E., Redford, P.S., Beebe, A.M., Bancroft, G.J., Young, D.B., and O'Garra, A. (2012). Blockade of IL-10 signaling during bacillus Calmette-Guérin vaccination enhances and sustains Th1, Th17, and innate lymphoid IFN-γ and IL-17 responses and increases protection to Mycobacterium tuberculosis infection. J. Immunol. *189*, 4079–4087.

Próchnicki, T., and Latz, E. (2017). Inflammasomes on the crossroads of innate immune recognition and metabolic control. Cell Metab. *26*, 71–93.

Rodríguez-Prados, J.C., Través, P.G., Cuenca, J., Rico, D., Aragonés, J., Martín-Sanz, P., Cascante, M., and Boscá, L. (2010). Substrate fate in activated macrophages: a comparison between innate, classic, and alternative activation. J. Immunol. *185*, 605–614.

Russell, D.G., Cardona, P.J., Kim, M.J., Allain, S., and Altare, F. (2009). Foamy macrophages and the progression of the human tuberculosis granuloma. Nat. Immunol. *10*, 943–948.

Selbach, M., Schwanhäusser, B., Thierfelder, N., Fang, Z., Khanin, R., and Rajewsky, N. (2008). Widespread changes in protein synthesis induced by microRNAs. Nature *455*, 58–63.

Sheedy, F.J. (2015). Turning 21: induction of miR-21 as a key switch in the inflammatory response. Front. Immunol. *6*, 19.

Sheedy, F.J., Palsson-McDermott, E., Hennessy, E.J., Martin, C., O'Leary, J.J., Ruan, Q., Johnson, D.S., Chen, Y., and O'Neill, L.A. (2010). Negative regulation of TLR4 via targeting of the proinflammatory tumor suppressor PDCD4 by the microRNA miR-21. Nat. Immunol. *11*, 141–147.

Shi, L., Salamon, H., Eugenin, E.A., Pine, R., Cooper, A., and Gennaro, M.L. (2015). Infection with Mycobacterium tuberculosis induces the Warburg effect in mouse lungs. Sci. Rep. *5*, 18176.

Su, X., Yu, Y., Zhong, Y., Giannopoulou, E.G., Hu, X., Liu, H., Cross, J.R., Rätsch, G., Rice, C.M., and Ivashkiv, L.B. (2015). Interferon-γ regulates cellular metabolism and mRNA translation to potentiate macrophage activation. Nat. Immunol. *16*, 838–849.

Tannahill, G.M., Curtis, A.M., Adamik, J., Palsson-McDermott, E.M., McGettrick, A.F., Goel, G., Frezza, C., Bernard, N.J., Kelly, B., Foley, N.H., et al. (2013). Succinate is an inflammatory signal that induces IL-1β through HIF-1α. Nature *496*, 238–242.

Tanner, L.B., Goglia, A.G., Wei, M.H., Sehgal, T., Parsons, L.R., Park, J.O., White, E., Toettcher, J.E., and Rabinowitz, J.D. (2018). Four key steps control glycolytic flux in mammalian cells. Cell Syst. *7*, 49–62.e48.

Terao, M., Fratelli, M., Kurosaki, M., Zanetti, A., Guarnaccia, V., Paroni, G., Tsykin, A., Lupi, M., Gianni, M., Goodall, G.J., and Garattini, E. (2011). Induction of miR-21 by retinoic acid in estrogen receptor-positive breast carcinoma cells: biological correlates and molecular targets. J. Biol. Chem. *286*, 4027–4042.

Weischenfeldt, J., and Porse, B. (2008). Bone marrow-derived macrophages (BMM): isolation and applications. CSH Protoc. *2008*, pdb.prot5080.

Wu, Z., Lu, H., Sheng, J., and Li, L. (2012). Inductive microRNA-21 impairs anti-mycobacterial responses by targeting IL-12 and Bcl-2. FEBS Lett. *586*, 2459–2467.

STAR★METHODS

KEY RESOURCES TABLE

REAGENT or RESOURCE	SOURCE	IDENTIFIER
Antibodies		
Anti-Mouse/Rat TNF alpha Functional Grade Purified Clone TN3-19.12	eBioscience	Cat# 16-7423-85, RRID: AB_469262
Armenian Hamster IgG Isotype Control Functional Grade Purified	eBioscience	Cat# 16-4888-85, RRID: AB_470172
murine IL-1b-neutralising antibody	R&D Systems	Cat# MAB4012, RRID: AB_2124619
goat IgG control	R&D Systems	Cat# AB-108-C, RRID: AB_354267
Human/Mouse/Rat Muscle Phosphofructokinase/PFKM Antibody	R&D Systems	Cat# MAB7687
Anti-b-actin	Sigma-Aldrich	Cat# A1978, RRID: AB_476692
Bacterial and Virus Strains		
Mycobacterium tuberculosis H37Ra	American Type Culture Collection	25177
Mycobacterium tuberculosis H37Rv	American Type Culture Collection	27294
Non-viable irradiated *Mycobacterium tuberculosis* strain H37Rv	BEI Resources	NR-49098
Heat-killed *Mycobacterium tuberculosis* H37Ra	Invivogen	tlrl-hkmt-50
Biological Samples		
Human bronchoalveolar lavage fluid	Patients attending for bronchoscopy at St James' Hospital, Dublin	n/a
Human buffy packs from donor blood	Obtained via the Irish Blood Transfusion Service	n/a
Chemicals, Peptides, and Recombinant Proteins		
Mouse IL-10 Recombinant Protein	eBioscience	14-8101-62
Mouse IFN gamma Recombinant Protein	eBioscience	BMS326
Ultrapure LPS from E.coli 0111:B4	InVivogen	tlrl-3pelps
Human IFN gamma Recombinant Protein	eBioscience	14-8319-80
2-Deoxy-D-glucose (2DG)	Sigma-Aldrich	**D8375**
Critical Commercial Assays		
Lactate Assay Kit	Sigma-Aldrich	MAK064
TaqMan miRNA Reverse Transcription Assays	Applied Biosystems	4366596
High-Capacity cDNA Reverse Transcription Kit	Applied Biosystems	4368814
Seahorse XF Cell Energy Phenotype Test Kit	Agilent	103325-100
Griess Reagent Nitrite Measurement Kit	Cell Signaling	13547
DCFDA/H2DCFDA Cellular Reactive Oxygen Species Detection Assay Kit	Abcam	ab113851
Mouse IL-1 beta ELISA Ready-SET-Go! Kit	eBioscience	5017185
Mouse TNF alpha ELISA Ready-SET-Go! Kit	eBioscience	5017331
Mouse IL-10 ELISA Ready-SET-Go! Kit, 2nd Generation	eBioscience	501125188
Phosphofructokinase Activity Colorimetric Assay Kit	Sigma-Aldrich	MAK093
Hexokinase Activity Colorimetric Assay Kit	Sigma-Aldrich	MAK091
Dual Luciferase Reporter Assay System	Promega	E1910
CytoTox 96 Non-Radioactive Cytotoxicity Assay	Promega	G1780
Human IL-1 beta ELISA Ready-SET-Go! Kit, 2nd Generation	eBioscience	15571087

(*Continued on next page*)

Continued

REAGENT or RESOURCE	SOURCE	IDENTIFIER
Experimental Models: Cell Lines		
HEK293T	gift of Prof. Cliona O'Farrelly, Trinity College, Dublin	n/a
RAW267.4	gift of Prof. Luke O'Neill, Trinity College, Dublin	n/a
L929	gift of Prof. Luke O'Neill, Trinity College, Dublin	n/a
Experimental Models: Organisms/Strains		
Whole-body deficient miR-21−/− mice generated from conditional knockout animals, described in Johnston et al., 2017.	Taconic/Artemis	C57BL/6 N.tac-Mirn21tm1698Arte
WT mice used for cell isolations	In-house colonies	C57BL/6JOlaHsd
Oligonucleotides		
miR-21/PFK-M TP morpholino (5′-AGCTTATTTTTAGGAA AACTCTTGAGTAGC-3′)	Gene Tools, designed by authors	n/a
miR-21/PFK-M control non-targeting morpholino 5′-ACC TTTTTTTTACGAAAACTGTTGAGTACC-3′)	Gene Tools, designed by authors	n/a
miRIDIAN microRNA Hairpin Inhibitor Negative Control #1	Dharmacon	IN-001005-01-05
miRIDIAN microRNA Hairpin Inhibitor hsa-miR-21-5p	Dharmacon	IH-300492-05-0005
miRIDIAN microRNA Mimic Negative Control #1	Dharmacon	CN-001000-01-05
miRIDIAN Hairpin Mimic hsa-miR-21-5p	Dharmacon	C-300492-03-0005
ON-TARGETplus Non-targeting siRNA #1	Dharmacon	D-001810-01-05
ON-TARGETplus Mouse Pfkm (18642) siRNA - Individual,	Dharmacon	J-065512-05-0005
TaqMan Pre-designed Gene Expression Assays	Applied Biosystems	see Table S1 for individual assay id's
Recombinant DNA		
hPFK-m 3′UTR linked firefly luciferase, hPFK-m 3′UTR sequence cloned into pEZX-MT06, annotated in ms as WT 3′UTR	Genecopoeia	n/a
Mutated hPFK-m 3′UTR linked firefly luciferase, mutant miR-21 site in hPFK-m 3′UTR sequence cloned into pEZX-MT06, annotated in ms as Mutant 3′UTR	Genecopoeia	n/a
pCMV-miR-21	Addgene	20381
pCMV-PL	Addgene	20783
Software and Algorithms		
FlowJo 7	FlowJo, LLC	https://www.flowjo.com/solutions/flowjo
PRISM 7	GraphPad	https://www.graphpad.com/
Microsoft Office Excel	Microsoft	https://products.office.com/en-au/excel
TargetScan v7.1	Bartel Lab, MIT	http://www.targetscan.org/vert_72/

LEAD CONTACT AND MATERIALS AVAILABILITY

Frederick J Sheedy (fsheedy@tcd.ie) is Lead Contact for this study. All unique reagents generated in this study (plasmids, oligonucleotides) are available from the Lead Contact without restriction.

EXPERIMENTAL MODEL AND SUBJECT DETAILS

Animals

miR-21-deficient mice were generated by Taconic using Cre-loxP technology to delete the miR-21 coding region downstream of *Tmem49*. Following successful deletion, mice were backcrossed further to obtain a full body *MiR-21*$^{-/-}$ line described by (Johnston et al., 2017). Uncrossed mice were used as *MiR-21*$^{+/+}$ controls (WT). Mice were bred and maintained under specific pathogen-free conditions. Mature (> 12 week) male and female mice were used for cell extractions (BMDM, AMs) and were age and sex-matched. Intra-peritoneal injection experiments were carried out on 12-week old male mice. Whole lung RNA from mice infected with Mtb H37

Rv (Erdman strain) was described in (Ouimet et al., 2016). All experiments were carried out under approval of the Health Products Regulatory Authority, Ireland and Trinity College Dublin Animal Research Ethics Committee.

Cell isolation and culture

BMDM were isolated as described in Weischenfeldt and Porse, 2008, and re-plated at day 7 post-differentiation at $1x10^6$ cell/mL in DMEM supplemented with 10% FBS and 5% L929-conditioned medium for experiments. Murine AM were isolated by bronchoalveolar lavage with ice-cold PBS via intratracheal insertion of a 20G IV catheter post-sacrifice. Cells were centrifuged from lavage fluid and plated in DMEM supplemented with 10% FBS and antibiotics (100 U/mL penicillin and 100 μg/mL streptomycin (Pen-Strep), counted and plated on plastic at $1x10^6$ cell/mL to allow adherence of macrophages. Non-adherent cells were washed away after 24 h. Human AM were retrieved at bronchoscopy after informed consent. Bronchoalveolar lavage fluid was filtered through a 100-μm nylon strainer (BD Bioscience) and centrifuged at 1,400 rpm for 10 min. Cells were resuspended at 5×10^5 cells/ml in RPMI-1640 culture media supplemented with human serum (Sigma), 50 μg/ml fungizone, and 50 μg/ml cefotaxime. Adherence purification of AM was performed; non-adherent cells were removed by washing after 24 h and experiments performed within 48 h. Cells were plated at $5x10^5$/ml. Work was approved by the Research Ethics Committee of St. James's Hospital. To generate human MDM, mononuclear cells were isolated from peripheral blood buffy coats obtained from the Irish Blood Transfusion Services (Dublin, Ireland) using density gradient centrifugation with Lymphoprep (Stem Cell Technologies). Cells were cultured on plastic in RPMI-1640 media supplemented with 10% human AB serum (Sigma-Aldrich) at 2×10^6/ml. Non-adherent cells were removed by washing every 2-3 days incubated for a total of 7 days to allow differentiation to macrophages prior to performance of experiments. Supply of human blood products from IBTS was approved by clinical indemnity to FJS. HEK293T cells were a gift from Clíona O'Farrelly (Trinity College Dublin) and were maintained in DMEM containing 10% FBS and Pen-Strep. RAW267.4 cells were a gift from Luke O'Neill (Trinity College Dublin) and were maintained in RPMI containing 10% FBS and Pen-Strep

Mycobacterium tuberculosis infections

Non-viable irradiated *Mycobacterium tuberculosis* (Mtb) strain H37Rv was obtained from the American Type Culture Collection (ATCC) (Manassas, VA) and prepared according to manufacturer's instructions. Mtb strains H37Ra and H37Rv were also obtained from ATCC and propagated in Middlebrook 7H9 medium to log phase. On the day of infection, bacteria in log-phase were pelleted by centrifugation and resuspended in DMEM. Bacterial pellets were de-clumped by passing through a syringe with an 25G needle several times. A single cell suspension was isolated by centrifuging the bacterial suspension at 800 rpm for 3 min. The supernatant of this spin was quantified by spectrophotometry (OD_{600nm}) and used to infect macrophages. Preliminary assessment of multiplicity of infection (MOI) was performed for each experiment and genotype to allow normalization for phagocytosis by infecting sample wells with varying amounts of resuspended Mtb for 3 h. For this, extracellular bacteria were removed by washing, cells fixed in 2% paraformaldehyde for 10 min and stained with Auramine O (Becton Dickinson) for acid-fast bacteria and with Hoechst 33358 (10 μg/ml; Sigma-Aldrich) for cell nuclei to allow determination of the number of bacilli per cell by observing slides under an inverted fluorescent microscope (Nikon TE 300). Macrophages were infected at an MOI of 5 bacilli per cell (unless otherwise stated) for 3 h, extracellular bacteria removed by collecting the supernatant which was then purified further by centrifugation at 13,000 rpm for 10 min to pellet extracellular bacteria. Bacteria-free media was returned to macrophages after washing in DMEM to remove extracellular bacteria. Baseline growth was assessed by lysing 3 h time-point in 0.1% Triton-X for 10 min. Serial dilutions were plated on 7H10 Middlebrook Agar in triplicate and colony-forming units enumerated after incubation at 37°C for 14 – 21 days after plating. For later growth measurements this lysate was combined with pelleted extracellular bacteria, obtained by centrifugation of supernatant. For experiments with viable Mtb, macrophage supernatants were sterilized through 20 nM filters before use. For intra-peritoneal injection of heat-killed Mtb (hk-Mtb), 12-week mice were injected with 750 μg hk-Mtb (InVivoGen) in 1 mL in endotoxin-free 1x PBS. 24 h post-injection mice were sacrificed and the peritoneal cavity flushed out with 2 mL PBS. Lavage fluid was collected and concentrated (Amicon Ultra Ultracel 3K columns) for ELISA.

METHOD DETAILS

Gene Expression analysis

RNA was extracted with the RNeasy Kit (QIAGEN), using a modified protocol to obtain small RNA species. For analysis of gene expression, cDNA was prepared with the High-Capacity cDNA Archive kit according to manufacturers' instructions (Applied Biosystems) and individual mRNAs were monitored with the following inventoried TaqMan assays (Applied Biosystems): mouse *18 s* (Mm04277571_s1), human *18S* (Hs03003631_g1), mouse arginase-1 (*Arg-1,* Mm00475988_m1), mouse hexokinase-2 (*Slc2a1,* Mm00443385_m1), human hexokinase 2 (*SLC2A1,* Hs00606086_m1), mouse Hypoxanthine-guanine phosphoribosyltransferase (*Hprt*, Mm01545399_m1), human *HPRT* (Hs02800695_m1), mouse interleukin-1β (*Il1b*, Mm00434228_m1), human *IL1B* (Hs01555410_m1), mouse interleukin-10 (*Il10*, Mm00439614_m1), human *IL10* (Hs00961622_m1), mouse lactate dehydrogenase A (LdhA, Mm01612132_g1), human *LDHA* (Hs01378790_g1), mouse inducible nitric oxide synthase (*Nos2*, Mm00440502_m1), mouse programmed cell death 4 (*Pdcd4*, (Mm01266062_m1), human *PDCD4* (Hs00377253_m1), mouse phosphofructokinase isoform liver (*Pfk-l*, Mm00435587_m1), human *PFKL* (Hs01036347_m1), mouse PFK isoform muscle (*Pfk-m*, Mm01309576_m1), human *PFKM* (Hs01075411_m1), mouse PFK isoform platelet (*Pfk-p*, Mm00444792_m1), human *PFKP* (Hs00737347_m1), mouse PTEN

(Mm00477208_m1), human phosphatase and tensin homolog (*Pten*, Hs02621230_s1), mouse *Pri-miR-21* (Mm03306822_pri), human pri-miR-21 (Hs03302625_pri), mouse tumor necrosis factor-α (*Tnf*, Mm00443258_m1) and human *TNF* (Hs00174128_m1). The AB7900HT platform (Applied Biosystems) was used for all PCR, performed in triplicate in FAST mode. Changes in expression were calculated by the change in threshold (ΔΔCT) method with *Hprt* or 18S as an endogenous control and were normalized to results obtained in untreated cells. For miRNA analysis, individual miRNA TaqMan assays for the endogenous reference small RNA RNU6B and miR-21 were performed according to the manufacturer's instructions RNU6B (conserved) (001093) and miR-21 (conserved) (Hs04231424_s1) (Applied Biosystems). For measurement of mycobacterial viability by qPCR, RNA and genomic DNA was isolated simultaneously and measured using; Mtb IS6100 genomic DNA specific probe (custom designed probe) and Mtb 16 s rRNA probes (Ba04230899_s1). For quantification, Mtb IS6100 expression in genomic DNA was normalized to bacterial housekeeping 16 s rRNA and macrophage 18 s rRNA expression in RNA samples and expressed relative to 3h post-infection using the ΔΔCT method.

Metabolic assays

Lactate concentration was measured in supernatants using the colorimetric Lactate Assay Kit (MAK064) (Sigma-Aldrich). Glucose concentration was measured using Glucose Assay Kit (ab65333) (Abcam). Enzyme activity was measured using kits from Sigma-Aldrich (Phosphofructokinase Activity Colorimetric Assay Kit MAK093 and Hexokinase Activity Colorimetric Assay Kit MAK091) according to manufacturer's instructions. Extracellular flux analyses were carried out using an XFe24 Extracellular Flux analyzer (Seahorse Biosciences) in Seahorse Media freshly supplemented with 10 mM glucose and 2 mM l-glutamine. Normalization for cell number was carried out with a Crystal Violet dye assay.

ELISA, Cell Viability, Nitrite and Intracellular ROS Assays

Cytokine concentration in supernatants were measured using sandwich ELISA READY-SET-GO kits from eBioscience according to the manufacturer's instructions. The following cytokines were assayed; mouse TNF (88-7324-77), mouse IL-10 (88-7105-77), mouse IL-1β (88-7013-77), human TNF (88-7346-77), human IL-10 (88-7106-77) and human IL-1β (88-7261-77. Cell viability was determined by measuring secreted lactate dehydrogenase using the CytoTox 96 Non-Radioactive Cytotoxicity Assay from Promega. Nitrite was measured in fresh supernatant using the Griess Reagent Nitrite Measurement Kit (Cell Signaling). Intracellular ROS were quantified using the DCFDA/H2DCFDA Cellular Reactive Oxygen Species Detection Assay Kit (ab113851) (Abcam).

Transfection and Plasmids

miR-21 specific miRNA inhibitors and mimics and non-targeting negative control molecules were obtained from Horizon Discovery/Dharmacon (miRIDIAN microRNA Hairpin Inhibitor Negative Control #1, miRIDIAN Hairpin Inhibitor hsa-miR-21-5p, miRIDIAN microRNA Mimic Negative Control #1 and miRIDIAN Hairpin Mimic hsa-miR-21-5p). Lipofectamine 2000 (Invitrogen) was used as a delivery agent. $1x10^6$ MDM or BMDM were transfected 7 days after maturation with RNA:Lipofectamine complexes at concentration of 50 nM RNA molecule, 2% Lipofectamine in serum-free OptiMEM media – left to complex at room temperature for 20 min prior to transfection. Cells were allowed to recover for 24 h before infection with Mtb. Luciferase activity was measured by transfecting HEK293T cells using GeneJuice (Merck) or RAW267.4 cells using Lipofectamine 2000 with a luciferase reporter plasmid miRNA 3′UTR target expression clone for Human PFKM (NM_000289.5) or a control mutated sequence (Genecopoeia) and assayed using the Dual-Luciferase kit (Promega). miR-21 was also overexpressed using pCMV-miR-21 or control vector pCMV-PL, both gifts from Bryan Cullen (Addgene plasmids 20381 and 20783). Target protection was achieved by transfecting cells using Lipofectamine 2000 to deliver the miR-21/PFK-M target protecting morpholino and control morpholino (5′-AGCTTATTTTTAGGAAAACTCTTGAGTAGC-3′) and 5′-ACCTTTTTTTTACGAAAACTGTTGAGTACC-3′) obtained from GeneTools (Oregon, USA). Mouse *Pfk-m* specific siRNA Horizon Discovery/Dharmacon (ON-TARGETplus Mouse *Pfk-m* (18642) siRNA) and BMDM were transfected using Lipofectamine 2000 to a top concentration of 50 nM and normalized with a non-targeting siRNA control 48h before further treatment/infection.

QUANTIFICATION AND STATISTICAL ANALYSIS

Statistical significance was assessed by one-way analysis of variance with multiple comparison tests using Prism 8 (Graph Pad software) or unpaired, two-tailed Student's t test for single comparison using Microsoft Excel. p values of less than 0.05 were considered significant and denoted by * or #. Information on replicates/error/significance are indicated in the figure legends

DATA AND CODE AVAILABILITY

This study did not generate any unique datasets or code